Soil Dynamics and Earthquake Engineering 31 (2011) 954–973

Contents lists available at ScienceDirect

Soil Dynamics and Earthquake Engineering

journal homepage: www.elsevier.com/locate/soildyn

Experimental study of the dynamic interaction between the foundation of the NEES/UCSD Shake Table and the surrounding soil: Reaction block response

J.E. Luco [a,*], O. Ozcelik [b], J.P. Conte [a], L.H. Mendoza [c]

[a] Department of Structural Engineering, University of California, San Diego, La Jolla, CA 92093-0085, USA
[b] Civil Engineering Department, Dokuz Eylul University, Tinaztepe Yerleskesi, Buca/Izmir 35160, Turkey
[c] Centro de Investigacion Cientifica y de Educacion Superior de Ensenada (CICESE), Ensenada, Baja California, Mexico

ARTICLE INFO

Article history:
Received 11 January 2010
Received in revised form
22 December 2010
Accepted 8 March 2011
Available online 3 April 2011

Keywords:
Soil–foundation interaction
Dynamics
Forced vibration tests
Experimental methods

ABSTRACT

An extensive experimental study of the dynamic interaction between the foundation block for the NEES/UCSD Large High Performance Outdoor Shake Table and the surrounding soil was conducted in 2003. The vibrations induced by the two NEES@UCLA large eccentric mass shakers were recorded at multiple stations within the reinforced concrete foundation block and on the surface of the surrounding soil up to distances of 270 m from the block. The present paper focuses on analysis of the data recorded within the reaction block including the average rigid body motion of the foundation and its dependence on frequency, and the deformation of the block for longitudinal (EW), transverse (NS), and torsional excitation. Comparison of the reaction block response during shaker induced vibrations with that for the much stronger actuator forces shows that linearity holds for the range of forces involved. Comparisons with analytical results for a simplified model of the foundation show good agreement between experimental and theoretical results.

1. Introduction

The construction of the foundation block for the NEES/UCSD Large High Performance Outdoor Shake Table (Fig. 1), which is part of the George E. Brown, Jr. Network for Earthquake Engineering Simulation (NEES) created a rare opportunity for an extensive experimental study of dynamic soil–foundation interaction effects. The large forces that the actuators of the shake table exert on the reaction block and the soil suggested the need to determine the induced ground motion in the vicinity of the table, as well as the need to evaluate the effects that any motion of the block itself would have on the control of the shake table. Although the shake table would operate initially with only longitudinal motion, it was designed to be readily upgradeable to six degrees of freedom. For this reason, it was necessary to estimate the response of the foundation block to at least longitudinal, transverse, and torsional excitation. To simulate the forces that the actuators would exert on the reaction block, the two large NEES/UCLA MK-15 eccentric mass shakers with a maximum force capacity of 0.445 MN (100,000 lb) each were mounted on the block at locations near the intended supports of the actuators. In tests conducted in October 21–24, 2003, the three-dimensional dynamic response at 19 locations on the reaction block; at 12 points on the foundation of the adjacent auxiliary building; and at 33 locations on the surface of the ground surrounding the shake table up to distances of over 270 m were recorded for longitudinal, transverse, and torsional excitation of the block with frequencies in the range from 0 to 20 Hz.

The first objective of the overall experimental study was to obtain dynamic ground motion data, and by inference geotechnical data, which will prove invaluable in the development of a future virtual model of the complete NEES/UCSD Shake Table Facility including a soil island surrounding the shake table and the adjacent soil pit, the reinforced concrete foundation block, the steel platen, the actuators and control system, and the test specimens [1]. The second objective of the study was to develop a body of dynamic high-quality response data on the foundation and surrounding soil that can be used to test and validate soil–structure interaction analysis methods and computer codes. In particular, the data would offer experimental information on the coupling through the soil between adjacent foundations. The study would complement the limited number of existing full-scale experimental studies of soil–structure interaction listed in the comprehensive review presented by Trifunac et al. [2]. The final objective was to validate the unconventional design of the NEES@UCSD foundation block in terms of its overall dynamic

* Corresponding author.
E-mail address: jeluco@ucsd.edu (J.E. Luco).

0267-7261/$ - see front matter
doi:10.1016/j.soildyn.2011.03.003

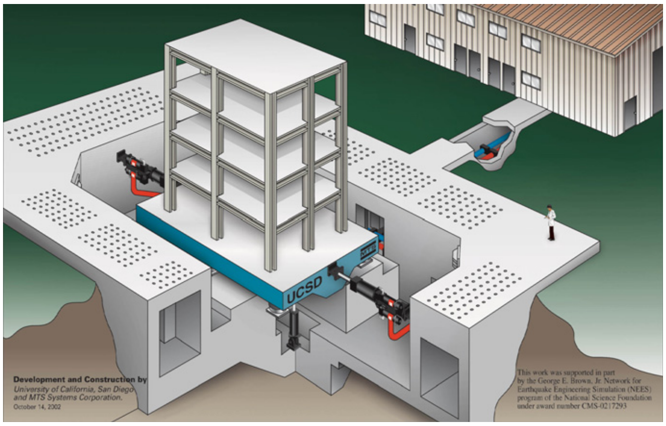

Fig. 1. Schematic representation of NEES/UCSD Shake Table.

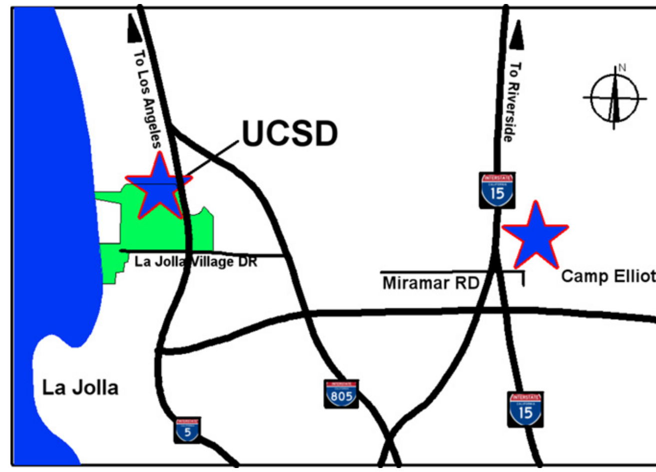

Fig. 2. Location of the NEES@UCSD facility.

response behavior, and to study experimentally the deformability of the foundation block and surrounding soils. The design of the NEES@UCSD foundation took advantage of the natural conditions at the site in terms of high soil stiffness to build a lighter and considerably less costly foundation, which resulted in a high characteristic frequency and a large effective damping ratio as opposed to the conventional design that relies on the use of massive foundations to achieve a low characteristic frequency.

The present paper presents the characteristics of the soil and foundation block and focuses on the dynamic response of the reaction block. The analysis of the attenuation of the ground motion on the soil surrounding the foundation will be presented in a companion paper [3]. The present paper includes detailed analysis of the average rigid body motion of the foundation and its dependence on frequency, and of the deformation of the block for longitudinal (EW), transverse (NS), and torsional excitation. Also, the response of the reaction block during shaker induced vibrations is compared with the response for the much stronger actuator forces. Finally, the experimentally based average rigid body motion of the block is compared with the theoretical response of a simplified model of the foundation.

The NEES/UCSD Shake Table is having a significant impact on the characterization of the seismic response of a variety of structures. In the last four years, full- or large-scale tests have been performed on a tall wind turbine [4], a segment of a 7-storey reinforced concrete building [5], a 3-storey pre-cast concrete parking structure [6], 3-storey reinforced concrete frames with masonry infills [7], brick veneers attached to wood and masonry structures [8], retaining walls placed on a large laminar soil shear box mounted on the shake table [9], large industrial-type metal structures, and large reinforced concrete bridge columns.

2. Characteristics of the foundation block and surrounding soil

2.1. Geological and geotechnical characteristics of the site

The site for the LHPOST occupies approximately 1.2 acres of land at the northwest end of the UCSD Englekirk Structural Engineering Research Center located in the Scripps Ranch area of San Diego, California, at a distance of about 15 km east of UCSD (Fig. 2). Topographically, the site is relatively flat with a mean elevation of 160 m (524 ft) above mean sea level (MSL). A gentle, natural slope bounds the site along the north, descending in elevation from 160 m (524 ft) MSL to an elevation of 148 m (484 ft) MSL at the bottom of an existing creek.

A field investigation including four exploratory borings drilled to depths varying from 1.8 to 21.6 m (6–71 ft) indicates that three general soil types underlie the site [10]. Top soils with a thickness varying from 0.6 to 0.9 m (2–3 ft) cover the site. These soils are characterized as firm, sandy clay with gravel and cobbles, and loose clayey sand with gravel and cobbles. Quaternary soils of the Linda Vista Formation underlie the top soils and extend to approximately 3.7 m (12 ft) below the existing elevation. The soils of this formation are characterized as very dense, clayey sands with gravel and cobbles. Tertiary soils of the Stadium Conglomerate were found beneath the soils of the Linda Vista Formation. These soils are characterized as very dense silty sand to sandy, cobbly gravel (Fig. 3).

Laboratory tests of undisturbed samples obtained from a boring that extended to a depth of 18.3 m (60 ft) resulted in an average in-place dry unit weight of 16.8 kN/m^3 (107.2 pcf) and an average moisture content of 10.25% for the Stadium Conglomerate. The corresponding values for the top soils were 18.0 kN/m^3 (114.6 pcf) and 8.65%, respectively. Results of a direct shear test on a sample taken at a depth of 4.25 m (14 ft) show a unit cohesion of 47.9 Pa (200 psf) and an angle of shear resistance of 38° [10]. The logs of borings separated by about 46 m (150 ft) (borings B-1 and B-3) show significant lateral differences between the soils at these two locations (Fig. 3). These differences become apparent in the Stadium Conglomerate at depths beneath 3.7 m (12 ft) from the surface.

Measurements of the shear-wave velocities at the site resulted in values of 185–305 m/s (600–1000 ft/s) for the Linda Vista Formation and 760 m/s (2500 ft/s) for the Stadium Conglomerate [11]. Earlier measurements at a site (East Campus Site) in a similar geologic setting resulted in values of 315 m/s down to a depth of 6 m and 560 m/s below that depth. The composite shear-wave velocity profile shown in Fig. 4 will be used later in the paper to compare analytical and experimental results.

2.2. Description of the foundation block

The reinforced concrete foundation block for the shake table is 33.12 m (108.67 ft) long, 19.61 m (64.33 ft) wide, and extends to a depth of 5.79 m (19 ft). A smaller central area of the foundation housing the hold down struts extends to a depth of 7.92 m (26 ft). To reduce the mass of concrete, the corners of the block have been truncated and its structure has been designed as a hollow tube along the perimeter (Figs. 5 and 6). The mass of the reaction block is 4.38×10^6 kg. A 6.10 m (20 ft) long tunnel with a 2.44 m $\times$ 2.44 m (8 ft $\times$ 8 ft) section connects the reaction block to the adjacent

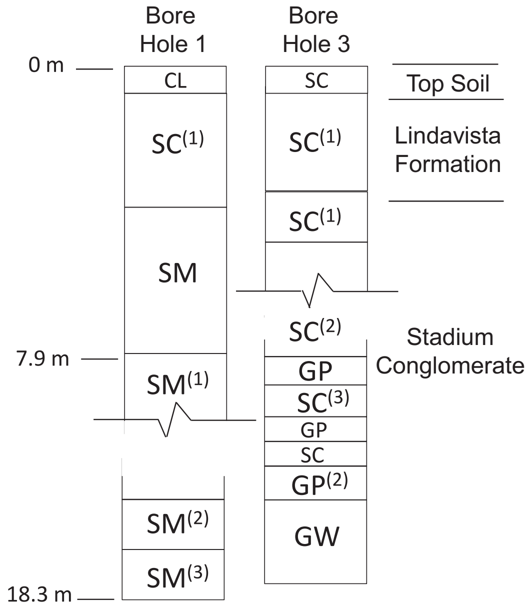

CL	Clay with sand
SC(1)	Clayey sand with gravel and cobbles
SM	Silty sand
SM(1)	Silty sand with gravel
SM(2)	Silty sand with gravel and cobbles, partially cemented
SM(3)	Silty sand uncemented

SC	Clayey sand
SC(2)	Clayey sand with abundant cobbles
GP	Cobbles and gravels
SC(3)	Clayey sand with gravels and cobbles
GP(2)	Gravel and cobbles with sand, boulders at 40 ft
GW	Cobbles, boulders and gravel

Fig. 3. Soil profiles at bore holes 1 and 3.

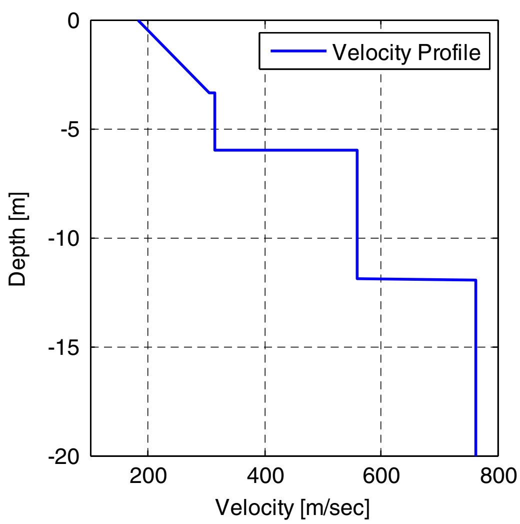

Fig. 4. Composite shear-wave velocity profile for the NEES@UCSD site.

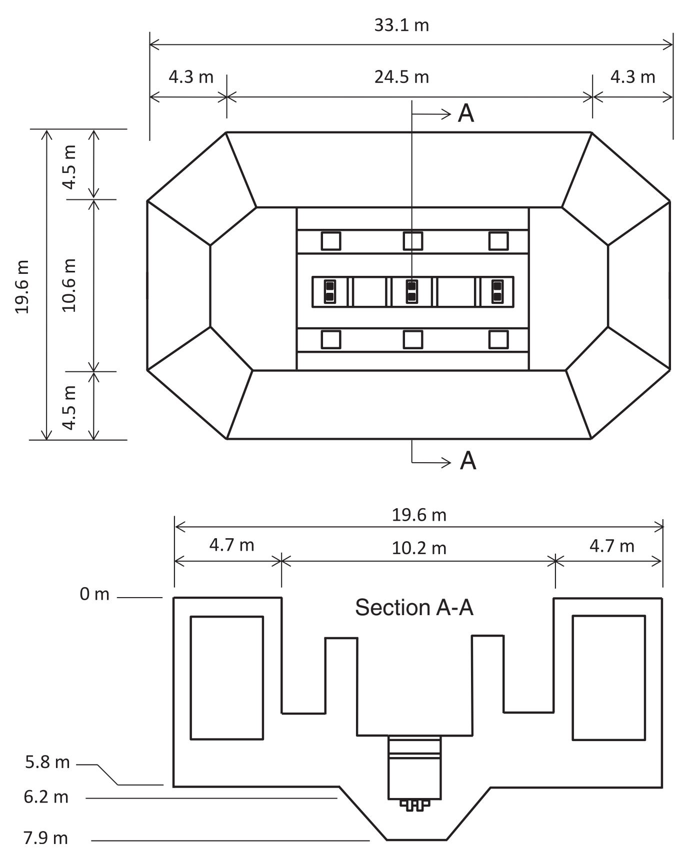

Fig. 5. Plan and cross-sectional view of the foundation block.

pump building, which is a 2-story structure with a partial basement. The pump building has plan dimensions of 15.5 m $\times$ 22.5 m and is founded at a depth of 3.5 m. A soil pit to the east of the shake table has plan dimensions of 14.6 m $\times$ 15.2 m and a maximum depth of about 5.8 m.

The reaction block supports the moving steel platen of the NEES Shake Table, which is 7.62 m (25 ft) wide, 12.19 m (40 ft) long, and has an effective mass of 144×10^3 kg [12,13]. In the initial phase of the facility, the motion of the table is unidirectional with a maximum stroke of 0.75 m, a peak horizontal velocity of 1.8 m/s, a peak horizontal acceleration of 4.2 g for bare table conditions and 1.2 g under a payload of 400 tons, an overturning moment capacity of 50 MN m, and a vertical payload capacity of 20 MN. The testing frequency range of the table is 0–33 Hz. In the initial phase, the system has two servo-controlled dynamic actuators with a combined total horizontal force capacity of 6.8 MN. The facility has an innovative vertical load/overturning moment bearing system including six pressure balanced

Fig. 6. MK-15 Shaker attached at the East end of the reaction block.

bearings and two hold down struts [14,15]. The forced vibration tests described here were conducted on the bare reinforced concrete reaction block (Fig. 6) before the platen, bearings, and actuators were installed.

3. Forced vibration tests

The forced vibration tests of the reaction block of the NEES/UCSD Shake Table were conducted using the equipment and personnel from the NEES/UCLA Earthquake Engineering Field Laboratory [16] supplemented with equipment and personnel from the Centro de Investigacion Cientifica y de Educacion Superior de Ensenada (CICESE), Mexico. Equipment from Incorporated Research Institutions for Seismology (IRIS) through the PASSCAL Instrument Center at New Mexico, was also used. The NEES/UCLA equipment included two MK-15 Shakers, 55 EpiSensor accelerometers, 17 Quanterra Q330 data loggers, and a mobile command center.

3.1. Characteristics of the MK-15 shakers

The two large NEES/UCLA MK-15 shakers (designed and constructed by ANCO Engineering, Boulder, Colorado) are uni-directional shakers with counter-rotating weights with an operating frequency range of 0–25 Hz, and a peak force of 445 KN (100,000 lb) each. Each of the two MK-15 shakers is fitted with two basket assemblies that counter-rotate in a horizontal plane. Each basket assembly consists of four segments (baskets # 1, 2, 3, 4) and a counterweight. The baskets have been designed to accommodate 5 cm × 10 cm × 20 cm (2 *in.* × 4 *in.* × 8 *in.*) steel bricks as a means of adjusting the total eccentricity (WR) of the system from 15.6 N m (138 lb in., empty baskets with counterweight) to 11,220 N m (99,295 lb in, baskets 1–4 filled with a total of 82 bricks) per basket assembly. Each shaker is driven by a 50HP motor, which is equipped with a new Vector drive (controller), which allows setting frequency to 0.1% FS accuracy over the 1–100% speed range. The controller also allows programming a step-sweep over a given frequency range and has a wireless control option. The system has a front panel digital display of frequency and a 1 pulse/revolution phase signal. In addition, a dual synchronized drive allows the two MK-15 shakers to run in phase lock (in-phase or out-of-phase). Within each shaker, the two rotating arms are synchronized mechanically.

Each MK-15 shaker with two counter-rotating eccentric weights produces a uni-directional sinusoidal force (F) that increases in direct proportion to the eccentricity (WR) and to the square of the rotating frequency (f (Hz)) as

$$F(t) = 2\left(\frac{WR}{g}\right)(2\pi f)^2 \sin(2\pi f t) \tag{1}$$

The amplitude of the force per shaker (in lb) can be written as

$$F(\text{lbs}) = 0.205\ WR\, f^2 \tag{2}$$

where the eccentricity per basket assembly WR is expressed in lb-inches.

In the tests described here, only the small basket (basket #1) was used with one or four bricks (laying flat) per basket. The corresponding eccentricities WR are 86 N m (761.4 lb in.) and 134 N m (1185.8 lb in.), respectively [17]. The resulting amplitudes of the force per shaker at 10 Hz are F=0.0694 MN (15,609 lb) for one brick and F=0.108 MN (24,301 lb) for 4 bricks. As shown in Fig. 6 the MK-15 shakers were attached to the East and West ends of the reaction block on the EW centerline and immediately above the reaction areas of the longitudinal actuators.

3.2. Sensors and data acquisition system

The instrumentation used in the experiments included 10 Triaxial EpiSensor Force Balance Accelerometers (NEES@UCLA), 45 Uniaxial EpiSensor Force Balance Accelerometers (NEES@UCLA), and 30 Uniaxial Mark Velocity Sensors (CICESE). The Kinemetrics EpiSensor accelerometers have a dynamic range of 140 dB (uniaxial) and 155 dB (triaxial), a bandwidth of DC to 200 Hz, a user selectable full-scale range that was set at ±2 g, and an output of ±20 V differential. The Mark L-4C 1.0 Hz geophone with a coil resistance of 5500 Ω has a transduction constant of 7.02 V/(in./s).

The uniaxial EpiSensor accelerometers were first bolted in triaxial packages to 20 cm × 20 cm × 0.64 cm (8 in. × 8 in. × 1/4 in.) aluminum plates that were secured to the ground by four 10 cm (4 in.) long corner spikes or bolted to the concrete of the foundations. The triaxial accelerometers were also attached to similar plates. The Mark seismometers were secured in place by sand bags.

The total number of acceleration and velocity channels recorded simultaneously amounted to 105 channels. In addition, 4 pulser channels (2 per MK-15 shaker) were used to record the location of the rotating baskets and to provide information to determine the phase of the harmonic shaker force. The 109 channels of data were acquired using 17 6-channel (NEES@UCLA) and 3 3-channel (2 UCSD, 1 IRIS) Quanterra Q330 data acquisition systems. The Kinemetrics Quanterra Q330 data loggers include a 24-bit A/D converter, a GPS receiver for time stamping for synchronization across multiple nodes, a local memory buffer, and a communication module. The system used had a sampling rate of 200 samples per second, a gain of one, an input range of 40 V peak-to-peak, a 135 dB dynamic range, and a time stamp (time synchronization) accuracy of < 0.1 ms.

In the NEES@UCLA field data acquisition system, the accelerometers (grouped in clusters of 6 channels each) transmit analog signals to the 6-channel Q330 data loggers in which they are digitized, time-stamped, and stored in a local memory buffer as data packets [16]. From there, the data packets are sent to the data concentration point using transmission control protocol/internet protocol (TCP/IP) via IEEE 802.11b long-range wireless radios. The data concentration point contains a Sun Microsystems Netra 120 server running Antelope data acquisition software [18] to centrally record data packets received from each of the various Quanterra Q330 nodes. Finally, the Antelope server in the data concentration point transmits wirelessly, using an orb2orb transfer protocol, all of the received data packets to a laptop computer inside the mobile command center also running Antelope software. The laptop computer was used to observe the experiment in real-time using the Antelope real-time monitoring (Antelope RTM) system.

3.3. Instrumentation of the reaction block and adjacent foundations

The reaction block was instrumented with 10 triaxial EpiSensor accelerometers (or packages of three uniaxial accelerometers) placed on the top surface of the block (RT1–RT10), 8 triaxial accelerometers (RB1–RB8) placed at the base of the block (5.18 m from the top), and one triaxial accelerometer (RB9) located at a sump at the center of the base of the block (6.2 m from top of block). The locations of the stations are shown in Fig. 7 and the corresponding coordinates are listed in Table 1.

The foundation of the pump building was instrumented with 6 triaxial arrangements of EpiSensor accelerometers (P1–P6). The tunnel connecting the reaction block and the pump building was instrumented with 2 triaxial arrangements of Mark seismometers (T1 and T2). Finally, the foundation of the Blast Simulator was instrumented with 4 triaxial arrangements of Mark seismometers (B1–B4). For reference, the three-dimensional motion of the soil at four stations (SSW, SSE, SNE, and SNW) adjacent to the reaction block was recorded with triaxial arrangements of Mark seismometers. The combined array of sensors included 31 triaxial stations on the foundations and four triaxial stations on the soil adjacent to the reaction block.

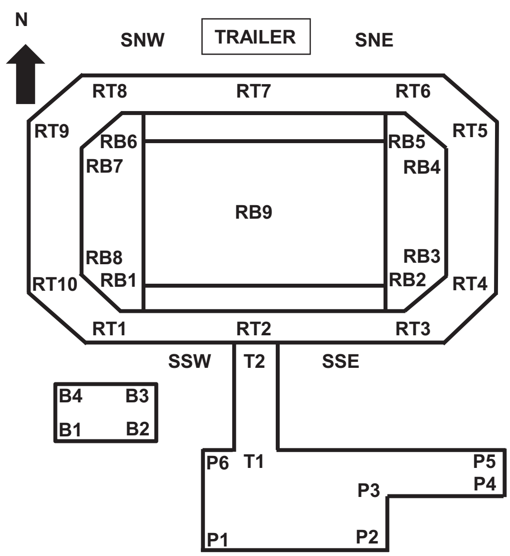

Fig. 7. Instrument locations on reaction block and the adjacent foundations.

Table 1
Coordinates of stations on reaction block (with respect to the center of base sump).

Station	x (m)	y (m)	z (m)
$RT1$	−10.20	−9.70	6.20
$RT2$	0.00	−9.70	6.20
$RT3$	10.20	−9.70	6.20
$RT4$	16.46	−4.98	6.20
$RT5$	16.46	4.98	6.20
$RT6$	10.20	9.70	6.20
$RT7$	0.00	9.70	6.20
$RT8$	−10.20	9.70	6.20
$RT9$	−16.46	4.98	6.20
$RT10$	−16.46	−4.98	6.20
$RB1$	−8.16	−4.98	1.02
$RB2$	8.16	−4.98	1.02
$RB3$	12.14	−2.77	1.02
$RB4$	12.14	2.77	1.02
$RB5$	8.16	4.98	1.02
$RB6$	−8.16	4.98	1.02
$RB7$	−12.14	2.77	1.02
$RB8$	−12.14	−2.77	1.02
$RB9$	0.00	0.00	0.00

3.4. Sequence of tests

A total of 109 sensors and 111 data acquisition channels were available for the experiment. This limitation made it necessary to conduct two sets of tests to satisfy the need to obtain the dynamic response of the foundation block and the surrounding soil at a large number of locations. In the first set of 8 tests presented here, most sensors were placed on the reaction block and on the foundations of the adjacent pump building and blast simulator. In the second set of 9 tests (to be discussed in a companion paper), most sensors were placed on linear arrays extending from the reaction block into the surrounding soil. The first sequence of tests is presented in Table 2. The tests included excitations in the EW (longitudinal) direction with one (Test 1) and two shakers acting in phase (Test 2), and two shakers out of phase (breathing mode, Test 3). Tests with excitation in the NS (transverse) direction included tests with one shaker (coupled NS translation and torsion, Test 6) with two shakers in phase (Tests 4 and 7) and two shakers out of phase (torsion, Tests 5 and 8). To check for linearity, several tests (Tests 5 and 8, 4 and 7) were conducted at two different levels of force. The forced vibration tests covered frequencies ranging from 1 to 18 Hz or 5 to 20 Hz depending on the level of force. Ambient vibration tests were conducted at the end of each set of tests for the two placements of sensors.

3.5. Data analysis

The first step for data analysis was to extract the data for each test from the Antelope data acquisition system. For each test, the acceleration responses from the Quanterra data loggers connected to the accelerometers on the top and bottom of the reaction block were extracted and stored in Matlab formats (.mat files), which are more convenient to use for further analysis. The second step was to detrend the raw data to remove the DC component of each signal and to filter the detrended data through a band-pass FIR filter with cut-in and cut-off frequencies of 0.5 and 25 Hz, respectively. These corner frequencies were chosen to envelope the minimum and maximum test frequencies. A high filter order of 512 was used to obtain sharp stop- and pass-band corners to prevent filtering out useful signal content. The third step was to calibrate the filtered signals recorded as units of "counts" to units of acceleration m/s^2 by multiplication by the coefficient $9.806/2^{22}$. The fourth step was to extract the time interval in which the steady state response of the reaction block for a particular

Table 2
Schedule of vibration tests.

Test no.	Excitation	Shaker(s)	Relative phase	Force level	Freq. range (Hz)
1	EW	E		4 Bricks	1–18
2	EW	E+W	0	4 Bricks	1–18
3	EW	E+W	180	4 Bricks	1–18
4	NS	E+W	0	4 Bricks	1–18
5	Torsion	E+W	180	4 Bricks	1–18
6	NS+Torsion	E		4 Bricks	1–18
7	NS	E+W	0	1 Brick	5–20
8	Torsion	E+W	180	1 Brick	7–20

excitation frequency was reached. For each frequency, these steady state portions were chosen to be at least 40 s long. The exact steady-state response frequency for each test frequency (i.e., intended frequency) was obtained by finding the peak frequency in the Fourier Amplitude Spectrum (FAS) plot of that particular response. Later, these exact response frequencies were used in a least-squares fit algorithm to find the amplitudes and phases of the steady state responses at different reaction block locations. The least-squares fits were applied to at least 10 s long signals processed by the data analysis procedure outlined above.

4. Response of the reaction block to longitudinal (EW) excitation

At the present time, the NEES/UCSD Shake Table operates one-directionally in the longitudinal (EW) direction. For this reason, it is important to consider first the response of the block to EW excitation with the two shakers acting in phase. In the case of Test 2 with four bricks in each basket, the combined harmonic total force exerted by the shakers at a frequency of 10 Hz has an amplitude of 0.216 MN (48,602 lb).

4.1. Accelerations at the top and base of the foundation block for EW excitation

The three-dimensional accelerations recorded at the top and base of the reaction block for an excitation frequency of 10 Hz during Test 2 are shown in Figs. 8 and 9, respectively. Fig. 8 shows a sample of the time histories of the *x*-East (column a), *y*-North (column b), and *z*-vertical (column c) components of acceleration for the 10 stations (*RT*1–*RT*10) at the top of the reaction block. Each frame in Fig. 8 includes the time histories of the accelerations at two stations symmetric with respect to the EW axis. Referring to the *x*-EW component (column a), it is apparent that: (i) the motion is symmetric with respect to the EW axis of the block, (ii) the central core (*RT*1, *RT*2, *RT*3, *RT*6, *RT*7, and *RT*8) translates almost as a rigid body, (iii) the accelerations at both ends of the block near the shakers (*RT*4 and *RT*5, *RT*9, and *RT*10) are larger than in the central core indicating out-of-plane deformation of the East and West walls, and (iv) the largest accelerations of about 0.39%*g* occur at the East end of the block adjacent to the (then) empty soil pit. Column (c) in Fig. 8 shows the vertical accelerations recorded on top of the block. The results indicate that: (i) the vertical accelerations are symmetric with respect to the EW axis but anti-symmetric with respect to the NS axis of the block, (ii) the amplitudes of the vertical accelerations increase with distance to the NS axis, indicating rocking of the reaction block about a NS axis, and (iii) the largest vertical accelerations of about 0.26%*g* occur at the East end of the block adjacent to the empty soil pit. Finally, the results for the *y*-North components of acceleration shown in column (b) indicate that: (i) the NS motion is mostly anti-symmetric with respect to the EW axis of the block, (ii) the NS motion at station *RT*2 located next to the tunnel is small suggesting a restraining effect by the tunnel, and (iii) the NS accelerations with a maximum amplitude of about 0.08%*g* are significantly smaller than the EW and vertical components.

Samples of the time histories of the *x*-East (column a), *y*-North (column b) and *z*-vertical (column c) components of acceleration

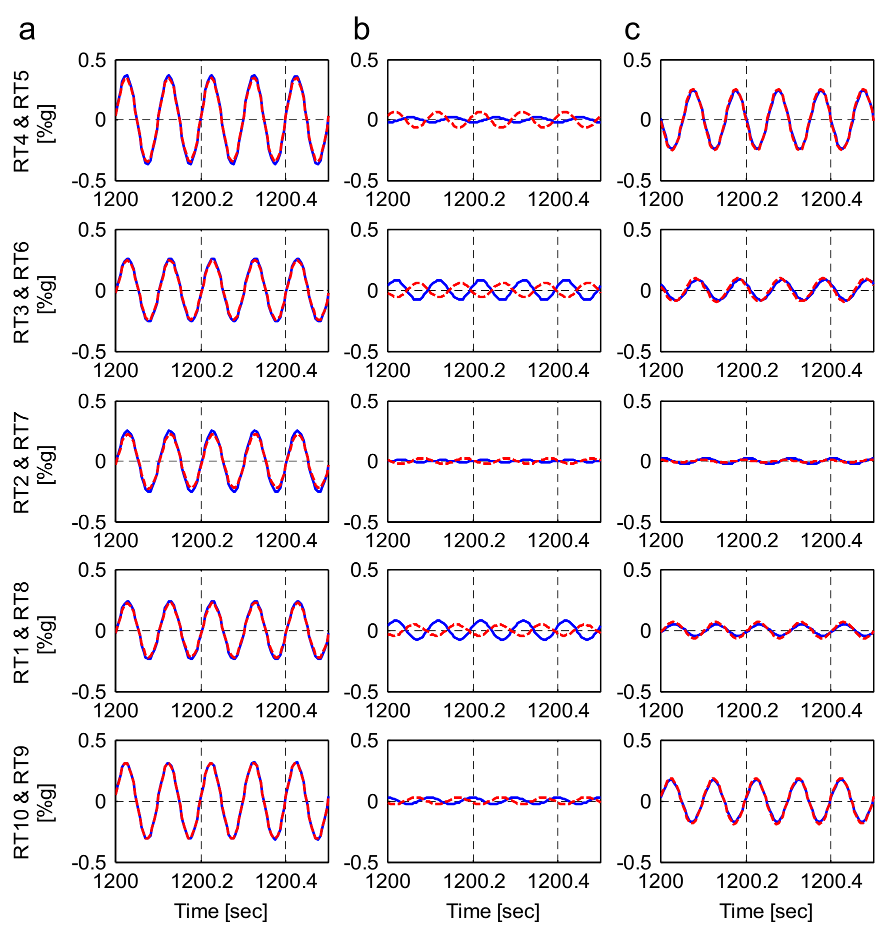

Fig. 8. Sample of time histories of the East (a), North (b), and vertical (c) acceleration components at the top of the reaction block (stations *RT*1–*RT*10) for EW excitation at 10 Hz (Test 2). In this figure and in the subsequent Figs. 9, 13, and 18, solid and dashed curves correspond, respectively, to stations along the southern and northern edges of the block.

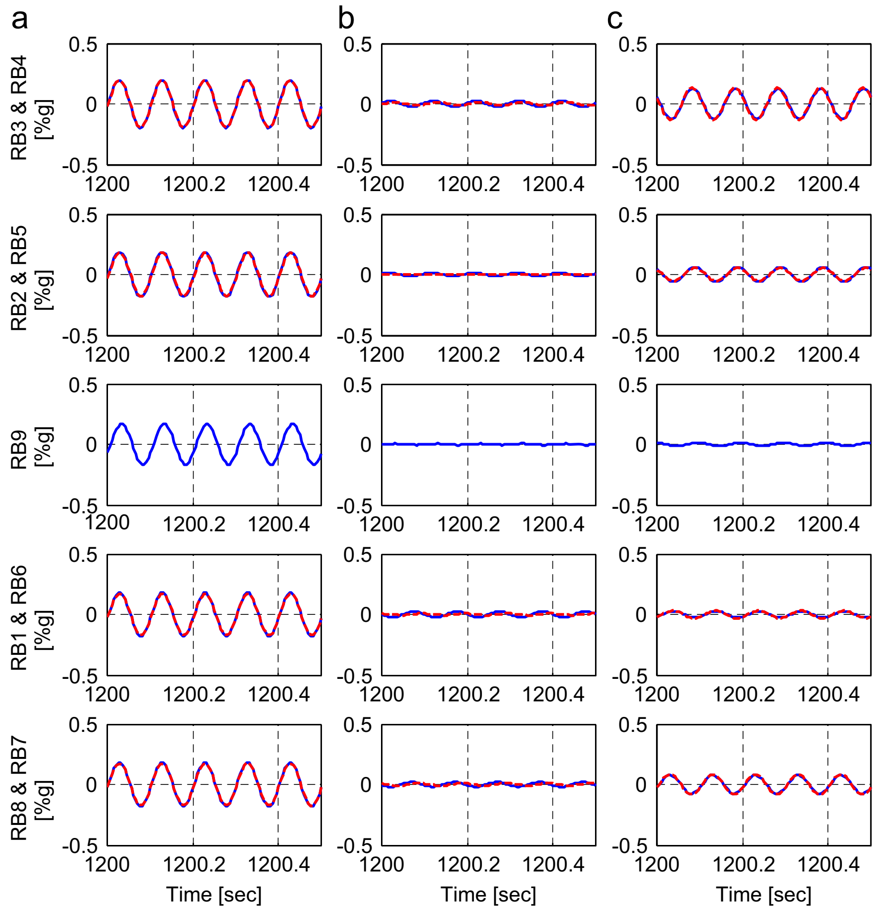

Fig. 9. Sample of time histories of the East (a), North (b), and vertical (c) acceleration components within the reaction block (stations *RB*1–*RB*9) for EW excitation at 10 Hz (Test 2).

for the 9 stations (*RB*1–*RB*9) within the reaction block are shown in Fig. 9. Again, each frame in Fig. 9 includes the time histories of the accelerations at two stations symmetric with respect to the EW axis. The response within the block shown in Fig. 9 is qualitatively similar to the response at the top of the block, but it shows more uniformity, suggesting less deformation at the lower levels of the block.

4.2. Deformation pattern of the foundation block for EW excitation

The displacement and deformation pattern of the reaction block for harmonic EW excitation with a frequency of 10 Hz is shown in Fig. 10a–d. Fig. 10a shows the initial geometry of the perimeter of the reaction block at ground level and the exaggerated deformed configuration in which the horizontal displacements have been scaled up by a factor of 10^6. Also shown are the 10 recording stations (filled squares) and their corresponding deformed positions (filled diamonds). The deformed perimeter was obtained by fitting a 5-parameter polynomial in x, y, and z to the observed displacements at all 19 stations.

The deformation of a lower level within the block is shown in Fig. 10b. The results in Fig. 10a and b show EW translation of the block and out-of-plane bending of the East and West walls and, to a lesser degree, of the North and South walls. The EW displacements of the East wall are larger than those on the opposite wall. This difference is related to the empty soil pit to the east of the block.

Figs. 10c and d show the amplitudes of the vertical displacements recorded at 19 stations plotted versus the (x, y) coordinates of the stations. Also shown in Fig. 10c and d is the vertical displacement pattern obtained by fitting a 5-parameter polynomial in x and y (but independent of z) to the recorded data at all 19 stations. The results in Fig. 10 confirm that the central portion of the block (*RT*1, *RT*3, *RT*6, and *RT*8) moves approximately as a rigid body, that there is bending of the East and West ends of the block, and that the vertical displacements recorded at the top of the block are consistent with those recorded within the block (i.e., the walls are essentially rigid in the vertical direction).

4.3. Frequency response functions

The amplitudes of the EW and vertical frequency response functions of the block are presented in Fig. 11a and b, respectively. The displacement amplitudes have been scaled linearly to a harmonic force of constant amplitude 6.8 MN, corresponding to the maximum force that the actuators can exert on the reaction block. The recorded accelerations were transformed to scaled displacements by multiplication through the factor$(6.8/0.216)(10/f)^2/(2\pi f)^2$. The amplitudes shown in Fig. 11a correspond to the averages of the EW components:

$$
\begin{aligned}
T3 &= (RT4+RT5+RT9+RT10)/4\\
T2 &= (RT1+RT3+RT6+RT8)/4\\
T1 &= (RT2+RT7)/2\\
B3 &= (RB3+RB4+RB7+RB8)/4\\
B2 &= (RB1+RB2+RB5+RB6)/4\\
B1 &= RB9
\end{aligned} \tag{3}
$$

The results in Fig. 11a indicate that: (i) the EW frequency response peaks at 10 Hz and has a peak amplification of about $2.6/2=1.3$, (ii) the average displacements *T*1 and *T*2 at the top of

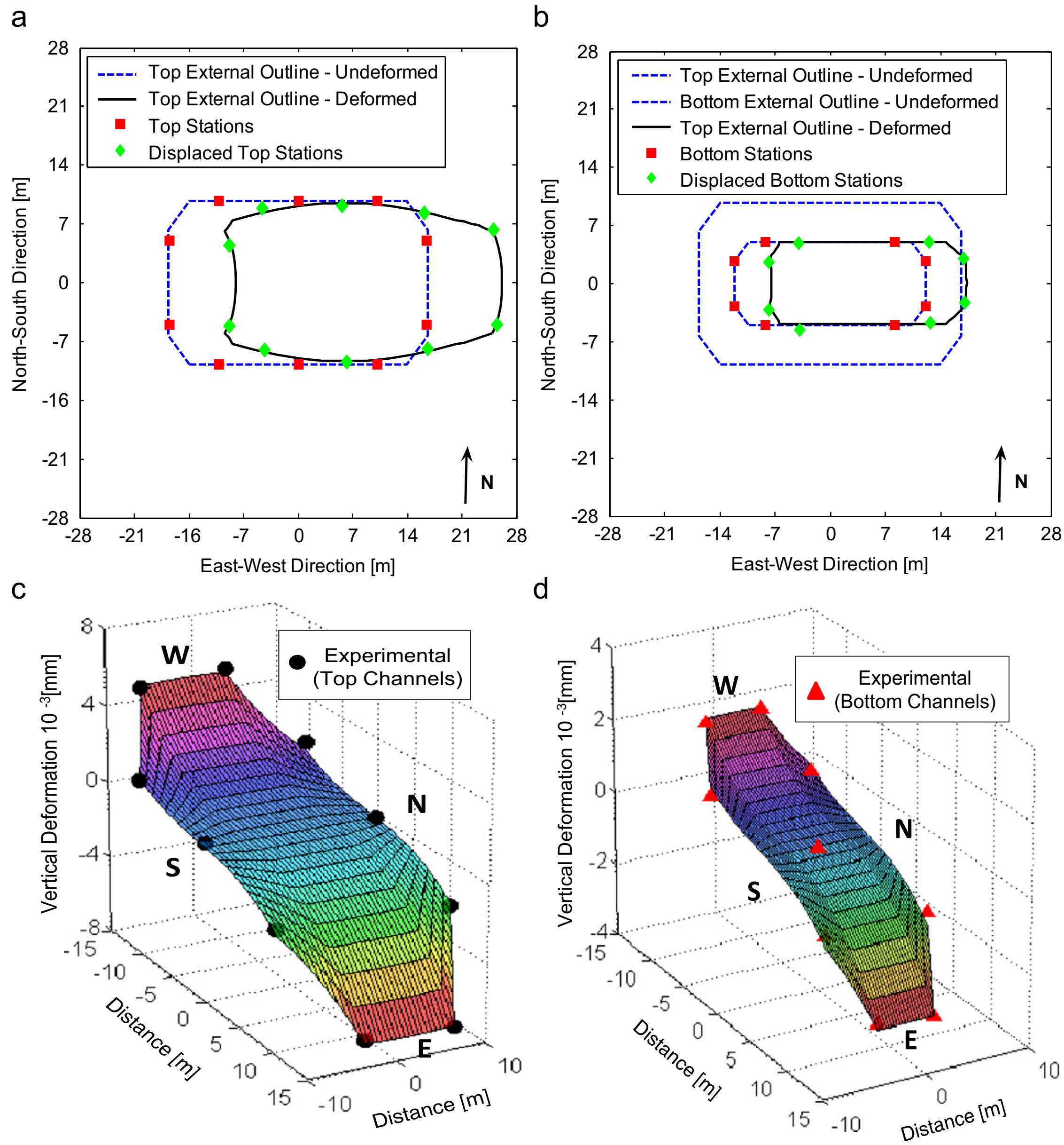

Fig. 10. Displacement and deformation of the reaction block for EW excitation using two shakers in phase at 10 Hz: horizontal deformation at the top (a) and within (b) the block, and distribution of vertical displacements on horizontal plane at the (c) top and (d) bottom of the block.

the block are very similar indicating that the central portion of the top of the block translates as a rigid body, (iii) the average displacement *T*3 at stations close to the East and West ends of the block is about 50% larger than the displacements *T*1 and *T*2 indicating out-of-plane deformation of the East and West end walls, (iv) the average *B*3 is only slightly larger than the average *B*2 indicating only a small deformation of the East and West areas within the block, and (v) the EW motions increase with elevation indicating the presence of a rocking component.

The amplitudes shown in Fig. 11b correspond to the averages of the vertical components:

$$\begin{aligned} VT3 &= (RT9+RT10-RT4-RT5)/4 \\ VT2 &= (RT1+RT8-RT3-RT6)/4 \\ VB3 &= (RB7+RB8-RB3-RB4)/4 \\ VB2 &= (RB1+RB6-RB2-RB5)/4 \end{aligned} \quad (4)$$

The results in Fig. 11b indicate that the amplitudes of the vertical displacements increase with horizontal distance to the NS axis of rotation at least for frequencies below 15 Hz. The distances to the NS axis from the stations at which the averages (*B*2, *T*2, *B*3, and *T*3) are calculated correspond to (8.16, 10.20, 12.14, and16.46) m, respectively. The amplitude ratios *T*3/*B*2, *B*3/*B*2, and *T*2/*B*2 at 10 Hz are 5.00, 2.43, and 1.67, respectively, while the ratios of the corresponding distances are 2.02, 1.49, and 1.25. This comparison indicates that there is vertical deformation of the reaction block in addition to rocking about the NS axis as shown in Fig. 10c and d.

The results in Fig. 11a and b for the averages *T*3 and *VT*3 of the motion at stations *RT*4, *RT*5, *RT*9, and *RT*10 indicate that the maximum scaled horizontal and vertical displacements for the maximum theoretical harmonic actuator force of 6.8 MN would be about 0.26 and 0.17 mm, respectively. These displacements are sufficiently small to have no effect on the control of the shake table, which relies on the assumption that the measured relative displacement of the platen with respect to the reaction block represents the absolute displacement of the platen. The peak

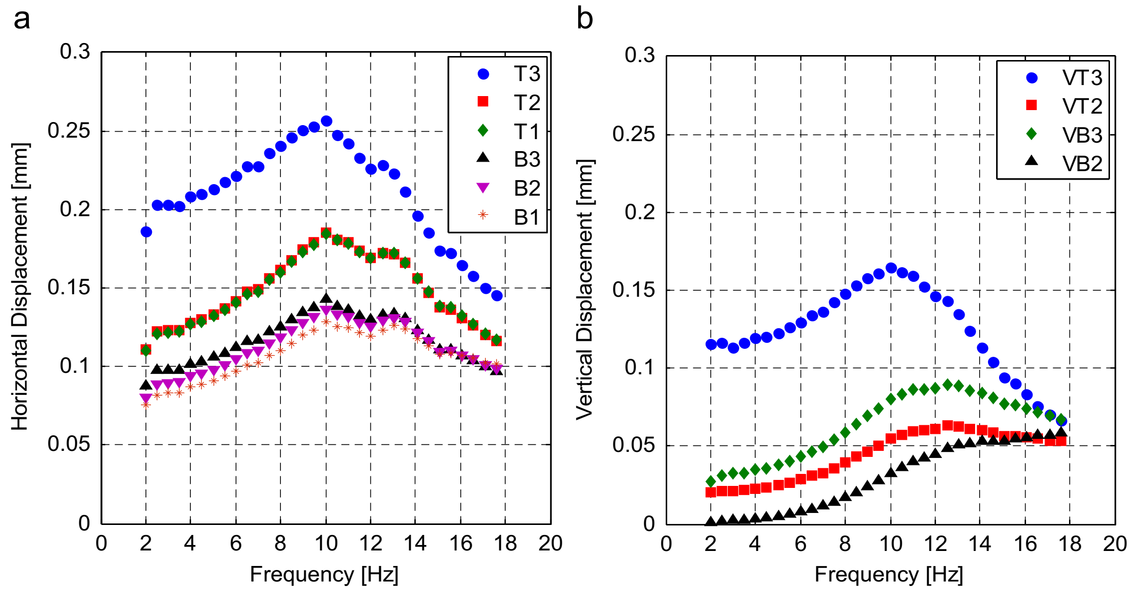

Fig. 11. Amplitudes of the EW (a) and vertical (b) frequency response functions of the reaction block for EW excitation. The results shown are based on Test 2 and correspond to scaled displacement amplitudes for a harmonic force of constant amplitude 6.8 MN.

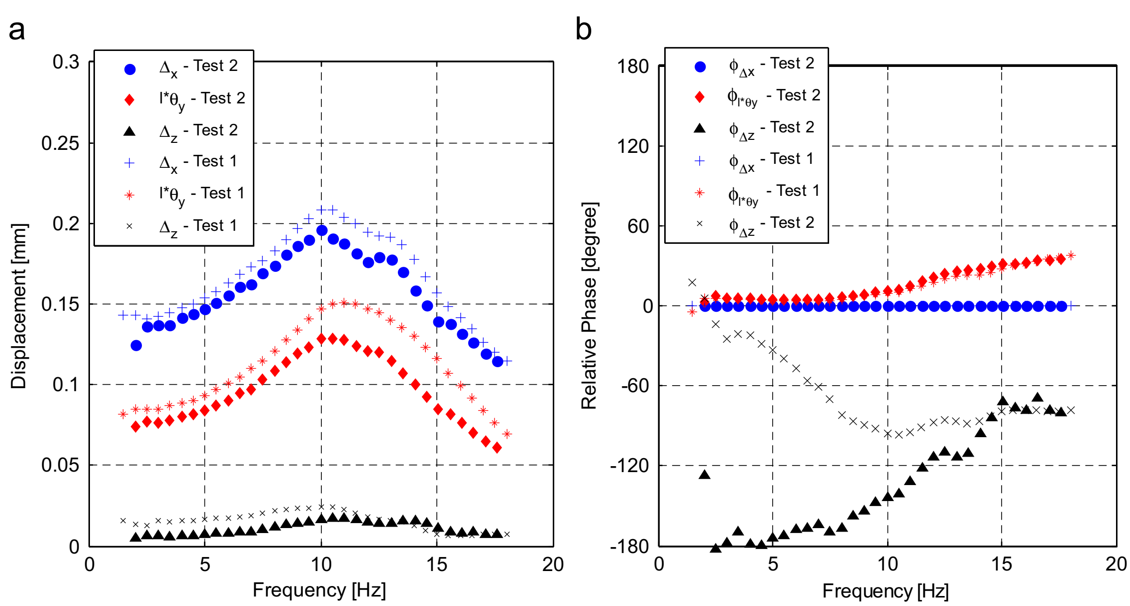

Fig. 12. (a) Amplitude and (b) relative phase of the frequency response function for the average EW, rocking, and vertical rigid-body motion of the reaction block subjected to EW excitation (Tests 1 and 2).

velocities on top of the reaction block of 1.63 cm/s (0.64 in./s) and 1.07 cm/s (0.42 in./s) are below the threshold of 2.54 cm/s (1 in./s) considered necessary to cause difficulties with mechanical equipment on the block. The maximum horizontal and vertical accelerations on top of the block would be 10.4%g and 6.9%g, respectively.

4.4. Estimates of average rigid-body motion

To facilitate comparisons with simple analytical models that assume that the block is rigid, we calculate next the average rigid-body motion of the reaction block. The average rigid-body motion is defined by the 6×1 vector:

$$\{\Delta_o\} = (\Delta_x, \Delta_y, \Delta_z, l\theta_x, l\theta_y, l\theta_z)^T \tag{5}$$

where $(\Delta_x, \Delta_y, \Delta_z)$ is the displacement of a reference point taken at the top center of the block, and $(\theta_x, \theta_y, \theta_z)$ are the rotations with respect to the coordinate axes (x-East, y-North, and z-up). The scaling factor $l = 16.56$ m was taken as the half-length of the reaction block. The vector $\{\Delta_o\}$ was determined through a least-squares fit to the recorded displacements $\{u_i\} = (u_{xi}, u_{yi}, u_{zi})^T$ at $N = 19$ stations on the block. The resulting expression for $\{\Delta_o\}$ is

$$\{\Delta_o\} = ([\alpha]^T[\alpha])^{-1}[\alpha]^T\{u\} \tag{6}$$

where

$$\{u\} = (\{u_1\}^T, \{u_2\}^T, \ldots, \{u_N\}^T) \tag{7}$$

$$[\alpha]^T = \begin{bmatrix} [\alpha_1]^T & [\alpha_2]^T & \cdots & [\alpha_N]^T \end{bmatrix} \tag{8}$$

and

$$[\alpha_i] = \begin{bmatrix} 1 & 0 & 0 & 0 & z_i/l & -y_i/l \\ 0 & 1 & 0 & -z_i/l & 0 & x_i/l \\ 0 & 0 & 1 & y_i/l & -x_i/l & 0 \end{bmatrix} \tag{9}$$

in which (x_i,y_i,z_i) are the coordinates of the ith station. The vector $\{\Delta_o\}$ was calculated in the time domain (step by step), and then the amplitudes and phases of the components $\Delta_x,\Delta_y,\ldots,l\theta_z$ were calculated for each test.

The scaled amplitude and the relative phase of the frequency response function for the average EW, rocking, and vertical rigid-body motion of the reaction block subjected to EW excitation with one (Test 1) and two (Test 2) shakers are presented in Fig. 12. The recorded accelerations during Test 2 were transformed to scaled displacements through multiplication by the factor $(6.8/0.216)(10/f)^2/(2\pi f)^2$. The corresponding scaling factor for Test 1 was twice as large. The linearly scaled amplitudes correspond to a harmonic force with constant amplitude of 6.8 MN. The most significant components of the average rigid-body motion are the EW translation and the rocking about the NS axis. The EW rigid body motion at the reference point at the top center of the block is consistent with the averages $T1$ and $T2$ of the motion of the top of the block shown in Fig. 11a. The obtained average rocking motion is consistent with the vertical motion in the central area of the block ($VT2$ in Fig. 11b at a distance of 10.2 m from the NS axis). There is also a small vertical motion of the center of the block due to asymmetry with respect to the NS axis associated with the empty soil pit and with lateral variations of soil properties. The transverse, torsional, and rocking (about the EW axis) components are very small and are not shown in Fig. 12.

The results in Fig. 12a show that the scaled amplitudes of the response during Test 1 (with one shaker) are proportionally slightly larger than the response during Test 2 (with two shakers). One explanation for this additional flexibility is that in Test 1 the shaker was located at the East end of the reaction block adjacent to the (then) empty soil pit. In Test 2, the additional West shaker is adjacent to well-compacted backfill. It is also possible that the two shakers in Test 2 were not perfectly in phase.

The pulsers on the shakers that were used to determine the phase of the harmonic force did not work properly during the tests. Consequently, the phase of the various response components with respect to the shaker force could not be obtained. Fig. 12b shows the relative phase of the rocking and vertical response with respect to the average EW rigid body displacement. The rocking response is essentially in phase with the EW displacement up to 10 Hz, while the average vertical displacement is 90–150° out of phase with respect to the EW displacement at 10 Hz.

5. Response of the reaction block to transverse (NS) excitation

To describe the response of the block to transverse (NS) excitation, it is convenient to start with Test 4 in which the two shakers placed at the East and West ends of the block acted in phase. In Test 4, with four bricks in each basket, the combined harmonic total NS force exerted by the two shakers at a frequency of 10 Hz had an amplitude of 0.216 MN (48,602 lb).

5.1. Accelerations at the top and base of the foundation block for NS excitation

The three-dimensional accelerations recorded at the top of the reaction block for an excitation frequency of 10 Hz during Test 4 are shown in Fig. 13. Fig. 13 shows a sample of the time histories of the East (column a), North (column b), and vertical (column c) components of acceleration for the 10 stations ($RT1$–$RT10$) at the top of the reaction block. Each frame in Fig. 13 includes the time histories of the accelerations at two stations symmetric with respect to the EW axis. Referring to the NS component (column b), it is apparent that: (i) the motion is symmetric with respect to the EW axis of the block, (ii) the accelerations at both ends of the block near the shakers ($RT4$ and $RT5$, $RT9$ and $RT10$) are larger than in the central core indicating bending or shear deformation of the block, and (iii) the largest accelerations of about 0.37%g occur at the East end of the block adjacent to the (then) empty soil pit. Column (c) in Fig. 13 shows the vertical accelerations recorded at the top of the block. The results indicate that: (i) the vertical accelerations are antisymmetric with respect to the EW axis and approximately symmetric with respect to the NS axis of the block, and (ii) the largest vertical accelerations of about 0.13%g occur at the East end of the block adjacent to the empty soil pit. Finally, the results for the East components of acceleration shown in column (a) indicate that: (i) the EW accelerations with a maximum amplitude of about 0.045%g are significantly smaller than the NS and vertical components and (ii) the EW motions at stations along the southern edge of the block ($RT10$, $RT1$, $RT2$, and $RT3$) are larger than those along the northern edge ($RT6$, $RT7$, $RT8$, and $RT9$).

Analysis of the accelerations recorded at the 9 stations ($RB1$–$RB9$) within the reaction block indicates that the response within the block is qualitatively similar to the response at the top of the block, but it shows more uniformity suggesting less deformation at the lower levels of the block.

5.2. Deformation pattern of the foundation block for NS excitation

The displacement and deformation pattern of the reaction block for harmonic NS excitation at a frequency of 10 Hz is shown in Fig. 14a–c. Fig. 14a shows the initial geometry of the perimeter of the reaction block at ground level and the exaggerated deformed configuration in which the horizontal displacements have been scaled up by a factor of 1.5×10^6. Also shown are the 10 recording stations (filled squares) and their corresponding deformed positions (filled diamonds). The deformed perimeter was obtained by fitting a 5-parameter polynomial in x, y, and z to the observed displacements at all 19 stations. The deformation of a lower level within the block is shown in Fig. 14b. The results in Fig. 14a and b show NS translation of the block, some torsion about a vertical axis, bending of the North and South walls, and, to a lesser degree, bending of the East and West walls. The NS displacement of the East wall and the EW displacement of the South wall are larger than those on the opposite walls. This difference and the torsional response are related to the unfilled soil pit to the east of the block and to the excavations during construction to both the east and south of the block.

The pattern of deformation in the vertical direction is illustrated in Fig. 14c and d, which shows the observed vertical displacements at all 19 stations together with a 5-parameter polynomial interpolation. The results show rocking of the East and West walls and anticlastic deformation of the slab.

5.3. Frequency response functions

After the NEES/UCSD Shake Table is upgraded to 6-DOF, the actuators arranged in V-shapes at the East and West ends of the block will exert NS forces on the reaction block with a maximum total value estimated at 3.4 MN. For comparison with the results for EW excitation, the results of Test 4 with a total force of 0.216 MN at 10 Hz were used to estimate the response of the reaction block to a harmonic force of 6.8 MN (double the expected

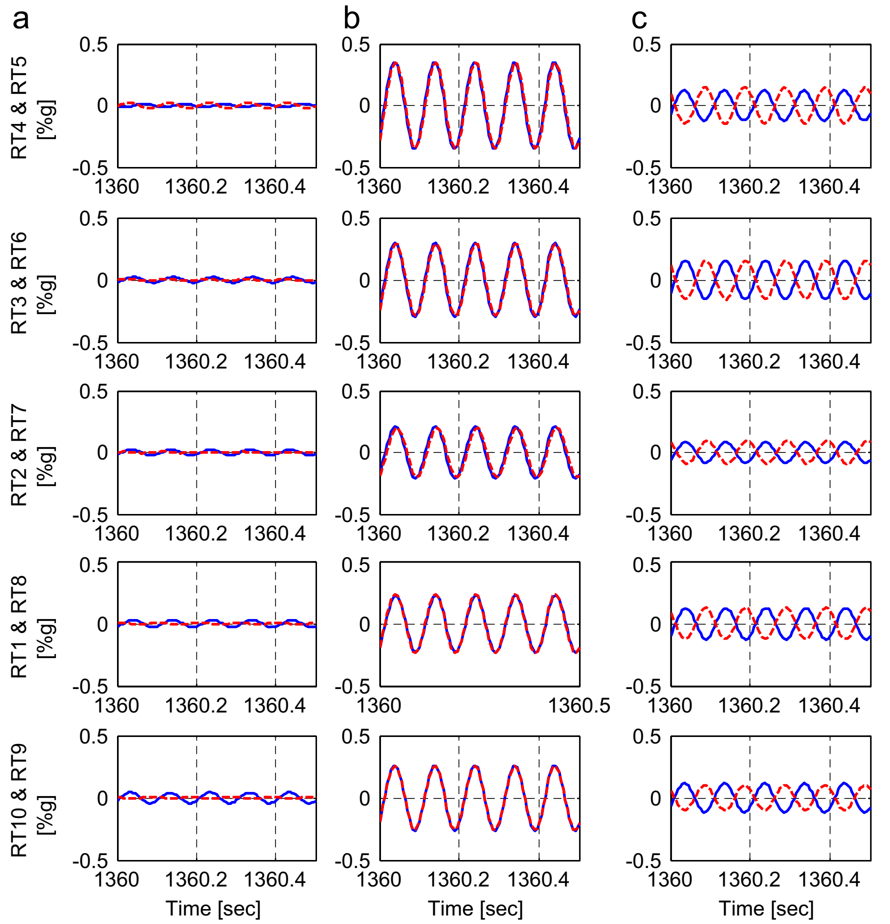

Fig. 13. Sample of time histories of the East (a), North (b), and vertical (c) acceleration components at the top of the reaction block (stations *RT*1–*RT*10) for NS excitation at 10 Hz (Test 4).

maximum NS force). For this purpose, the recorded accelerations were transformed into displacements and then scaled to a NS excitation force of 6.8 MN independent of frequency by use of the factor $(6.8/0.216)(10/f)^2/(2\pi f)^2$, where f is the cyclic frequency (Hz). The amplitudes of the resulting NS and vertical frequency response at different locations in the block are presented in Fig. 15a and b, respectively. The amplitudes shown in Fig. 15a correspond to the averages of the NS components:

$$\begin{aligned}
T3 &= (RT4+RT5+RT9+RT10)/4\\
T2 &= (RT1+RT3+RT6+RT8)/4\\
T1 &= (RT2+RT7)/2\\
B3 &= (RB3+RB4+RB7+RB8)/4\\
B2 &= (RB1+RB2+RB5+RB6)/4\\
B1 &= RB9
\end{aligned} \tag{10}$$

The terms $T1$, $T2$, and $T3$ correspond to average NS motions at the top of the block at distances of 0, 10.2, and 16.5 m from the NS centerline. The terms $B1$, $B2$, and $B3$ correspond to average NS motions within the block at distances of 0, 8.2, and 12.1 m from the NS centerline.

The results in Fig. 15a indicate that: (i) the NS frequency response near the East and West walls ($T3$) peaks at 10 Hz and has a peak amplification of about $0.205/0.15=1.4$, (ii) near the NS axis of the block and at the bottom of the block there is a second peak at 14 Hz, (iii) the average displacements $T2$ and $T3$ at the top of the block are very different from $T1$ indicating localized deformations at the east and west ends of the block, (iv) the averages at the base of the block also show localized deformation near the East and West walls, and (v) the NS motions increase with elevation indicating the presence of a rocking component and bending of the North and South walls.

The amplitudes shown in Fig. 15b correspond to the averages of the vertical components:

$$\begin{aligned}
N1 &= (RT6+RT7+RT8)/3\\
N2 &= (RT5+RB5+RB6+RT9)/4\\
N3 &= (RB4+RB7)/2\\
S3 &= (RB3+RB8)/2\\
S2 &= (RT4+RB2+RB1+RT10)/4\\
S1 &= (RT1+RT2+RT3)/3
\end{aligned} \tag{11}$$

The terms N1–S1, N2–S2, and N3–S3 correspond to averages of stations at distances of 9.70, 4.98, and 2.77 m from the EW axis of the block. The results in Fig. 15b indicate that the amplitudes of the vertical displacements increase with horizontal distance to the EW axis of rotation, that the motions are approximately antisymmetric with respect to the EW axis, and that the peak response occurs at about 13 Hz.

The results in Fig. 15a and b indicate that the maximum scaled horizontal and vertical displacements for the maximum nominal harmonic actuator force of 3.4 MN would be 0.1 and 0.05 mm, respectively.

5.4. Estimates of average rigid-body motion

The scaled amplitude and the relative phase of the average NS, rocking, and vertical rigid-body motion of the reaction block subjected to NS excitation with two shakers with four bricks per basket (Test 4) were determined by the procedure described

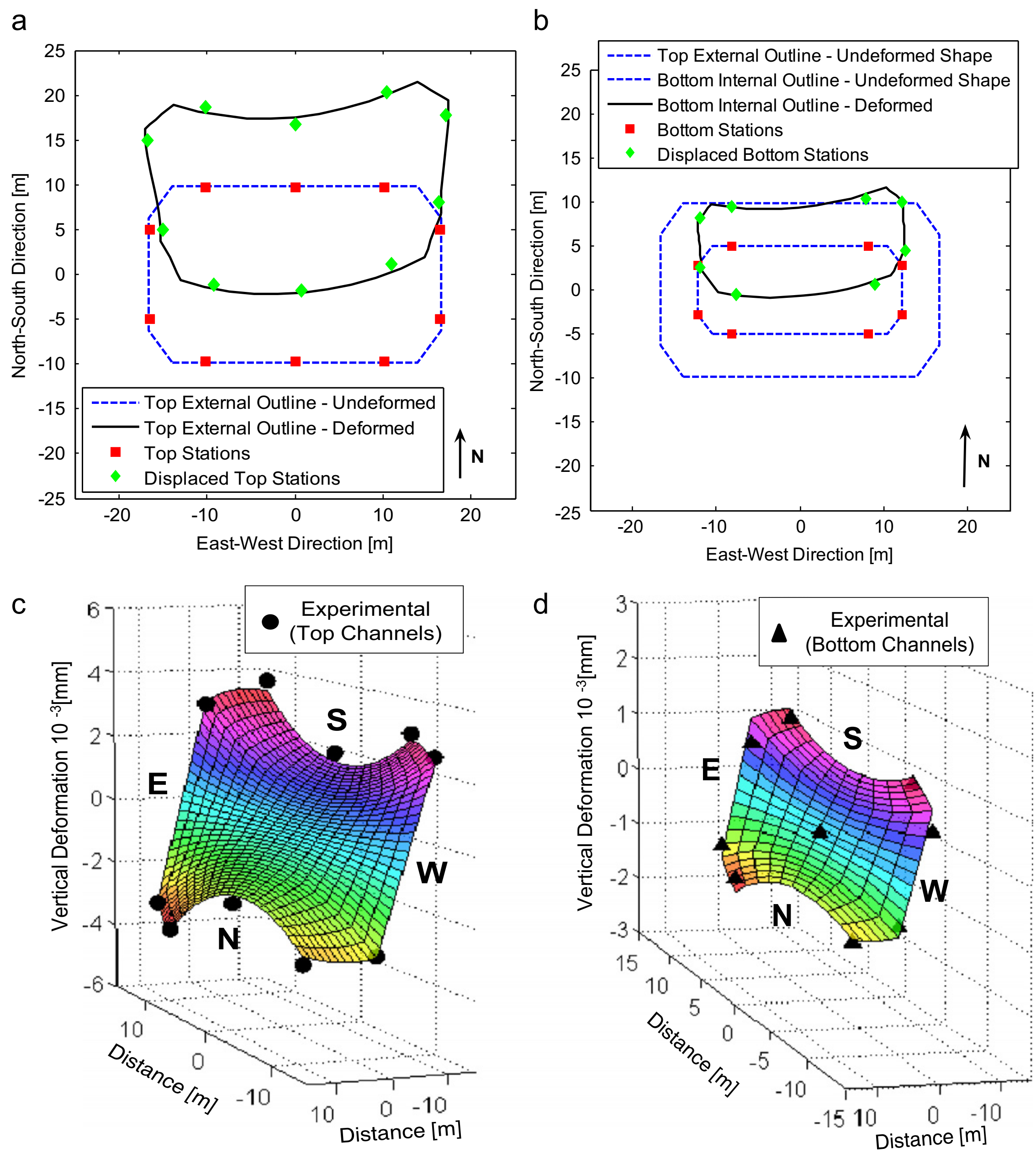

Fig. 14. Displacement and deformation of the reaction block at the top of (a) and within (b) the block for NS excitation at 10 Hz, and distribution of vertical displacements on horizontal plane at the top (c) and bottom (d) of the block.

in Section 4.3 and are presented in Fig. 16. The recorded accelerations during Test 4 were transformed to scaled displacements through multiplication by the factor$(6.8/0.216)(10/f)^2/(2\pi f)^2$. The linearly scaled amplitudes correspond to a harmonic force with constant amplitude of 6.8 MN. The most significant components of the average rigid-body motion are the NS translation and the rocking rotation about the EW axis. The NS rigid-body motion at the reference point at the top center of the block is consistent with the average of the terms $T1$, $T2$, and $T3$ shown in Fig. 15a for the motion of the top of the block. The rocking motion is also consistent with the vertical motion at the north and south walls (N3 and S3 in Fig. 15b). There is a small torsional component due to asymmetry with respect to a vertical axis associated with the empty soil pit, with lateral variations of soil properties, and with possible imperfect synchronization of the two shakers. The vertical, longitudinal, and rocking (about the NS axis) components are very small and are not shown in Fig. 16.

Fig. 16b shows the relative phase of the rocking and torsional response with respect to the average NS rigid-body displacement response. The rocking response is approximately 180° out of phase with respect to the NS displacement, while the torsional response is approximately in phase with respect to the NS displacement at 10 Hz.

5.5. Test of linearity

The results of Test 4 with a total NS force of 0.216 MN at 10 Hz (four bricks per basket) and Test 7 with a total force of 0.139 MN at 10 Hz (one brick per basket) were used to check the linearity of the system. The recorded accelerations were transformed into displacements and then scaled to a harmonic excitation force of 6.8 MN independent of frequency. Comparisons of the normalized NS displacements at stations $RT7$ and $RB9$ and of the normalized vertical displacement at station $RT7$ for the two tests are presented in Fig. 17.

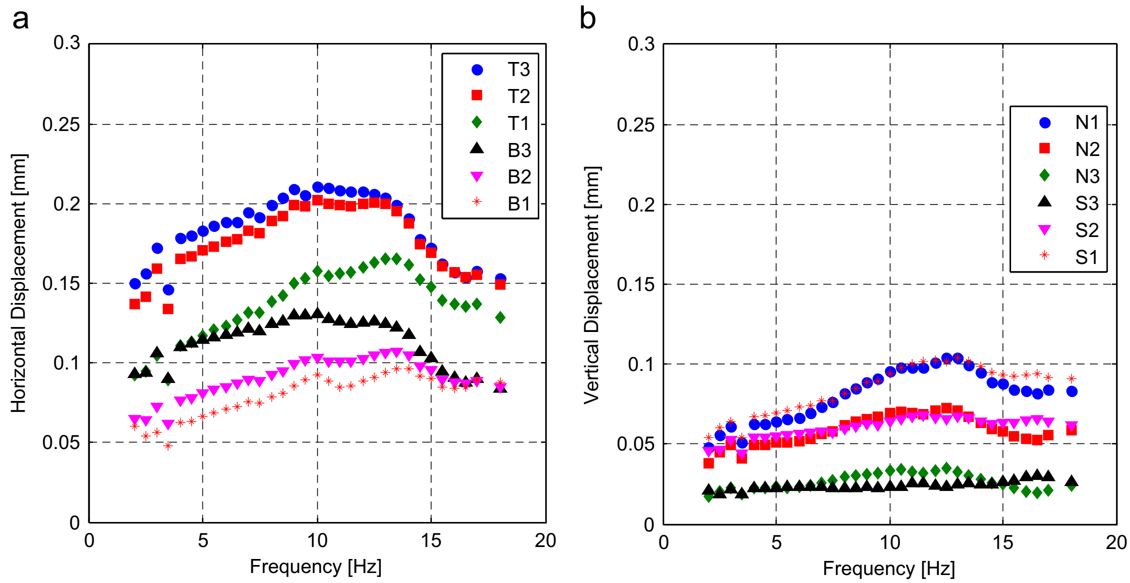

Fig. 15. Amplitudes of the NS (a) and vertical (b) frequency response functions of the reaction block for NS excitation. The results shown are based on Test 4 and correspond to scaled displacement amplitudes for a harmonic force of constant amplitude 6.8 MN.

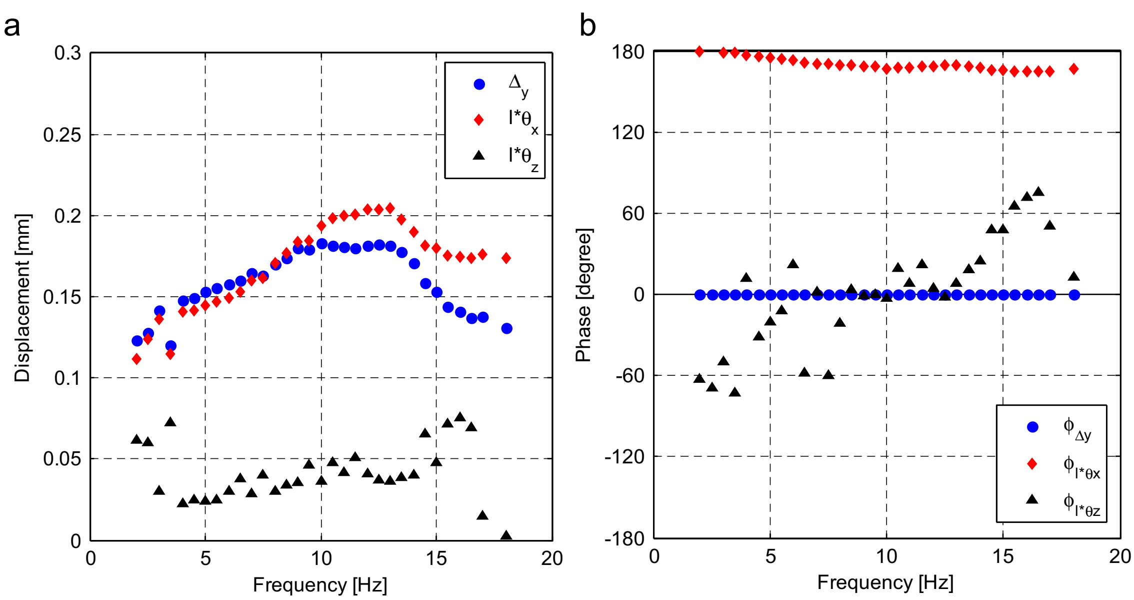

Fig. 16. (a) Amplitude and (b) relative phase of the frequency response functions for the average NS, rocking, and torsional rigid-body motion of the reaction block subjected to NS excitation (Test 4).

These results show that the scaled amplitudes for the response during Test 7 (with one brick per basket) are proportionally only slightly larger than the response during Test 4 (with four bricks per basket).

6. Response of the reaction block to torsional excitation

The response of the block to torsional excitation was studied in Tests 5 and 8 in which the two shakers placed at the East and West ends of the block acted in opposite NS directions. In Test 5 with four bricks in each basket, the harmonic NS force exerted by each shaker at a frequency of 14.5 Hz had an amplitude of 0.227 MN (51,093 lb) and the corresponding total torque about the vertical axis was 6.50 MN m (as the distance between the centers of the two shakers was 28.6 m). Test 8 with a force of 0.146 MN (32,817 lb) per shaker (one brick per basket) at 14.5 Hz had a total torque of 4.18 MN m at the same frequency.

6.1. Accelerations at the top and base of the foundation block for torsional excitation

The three-dimensional accelerations recorded at the top of the reaction block during Test 5 for an excitation frequency of 14.5 Hz are shown in Fig. 18. Fig. 18 shows a sample of the time histories of the East (column a), North (column b), and vertical (column c) components of acceleration for the 10 stations (*RT*1–*RT*10) at the top of the reaction block. Each frame in Fig. 18 includes the time histories of the accelerations at two stations symmetric with respect to the EW axis. Referring to the NS component (column b), it is apparent that: (i) the motion is symmetric with respect to the EW axis of the block, (ii) the accelerations at both ends of the block near the shakers (*RT*4 and *RT*5, *RT*9 and *RT*10) are larger than in the central core indicating torsion and bending or shear deformation of the block, and (iii) the largest accelerations of about 2.17%*g* occur at the East end of the block adjacent to the (then) empty soil pit. Column (c) in Fig. 18 shows the

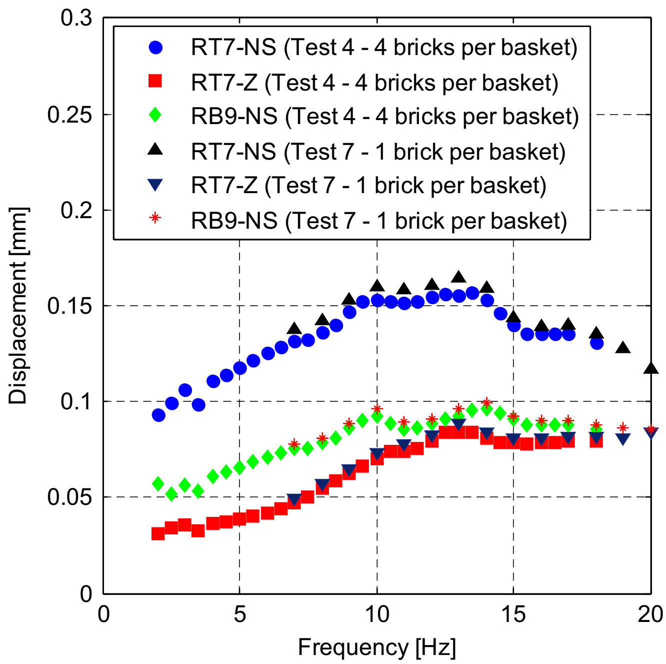

Fig. 17. Test of linearity for NS excitation based on Tests 4 and 7.

vertical accelerations recorded at the top of the block. The results indicate that: (i) the vertical accelerations are anti-symmetric with respect to both the EW and NS axes, and (ii) the largest vertical accelerations of about 0.78%*g* occur at the East end of the block adjacent to the empty soil pit. Finally, the results for the East components of acceleration shown in column (a) indicate that: (i) the EW accelerations with maximum amplitude of about 0.52%*g* are smaller than the NS and vertical components and (ii) the EW motions at stations near the center of the block are larger than those near the East and West ends. The response at the 9 stations (*RB*1–*RB*9) within the reaction block is qualitatively similar to the response at the top of the block.

6.2. Deformation pattern of the foundation block for torsional excitation

The displacement and deformation patterns of the reaction block for torsional excitation (Test 5) at a frequency of 14.5 Hz are shown in Fig. 19a–c. Fig. 19a shows the initial geometry of the perimeter of the reaction block at ground level and the (exaggerated) deformed configuration in which the horizontal displacements have been scaled up by a factor of 0.5×10^6. Also shown are the 10 recording stations (filled squares) and their corresponding deformed positions (filled diamonds). The deformed perimeter was obtained by least-square fitting a 5-parameter polynomial in *x*, *y*, and *z* to the observed

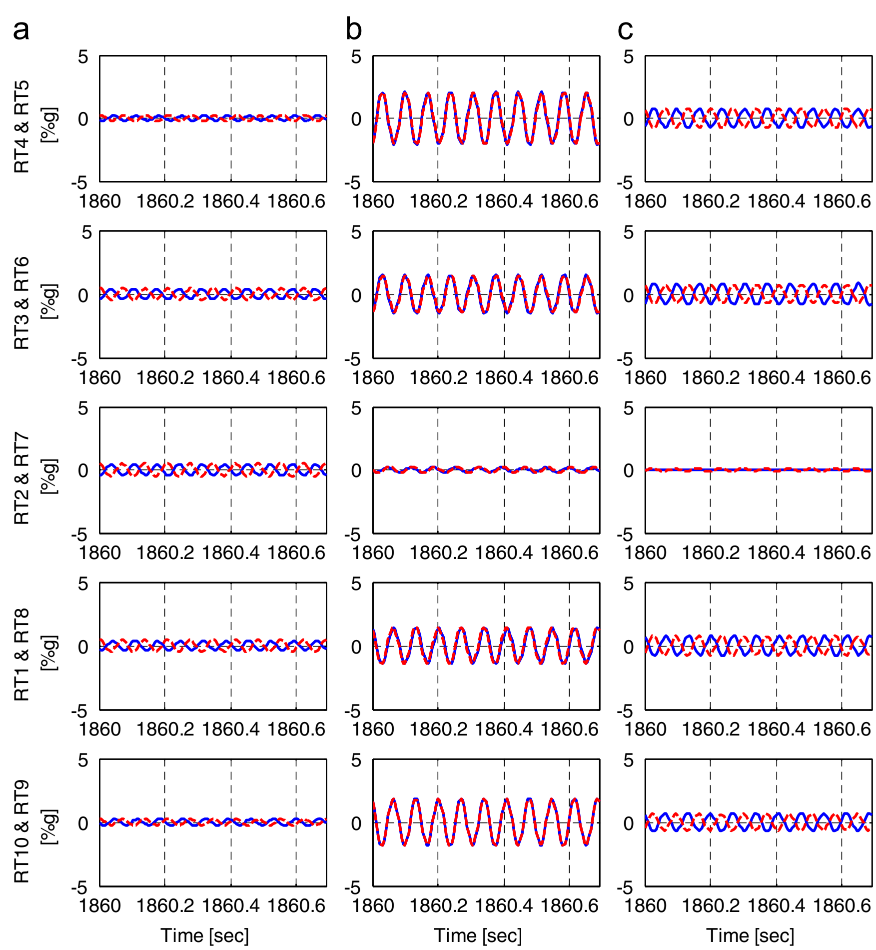

Fig. 18. Sample of time histories of the East (a), North (b), and vertical (c) acceleration components at the top of the reaction block (stations *RT*1–*RT*10) for torsional excitation at 14.5 Hz (Test 5).

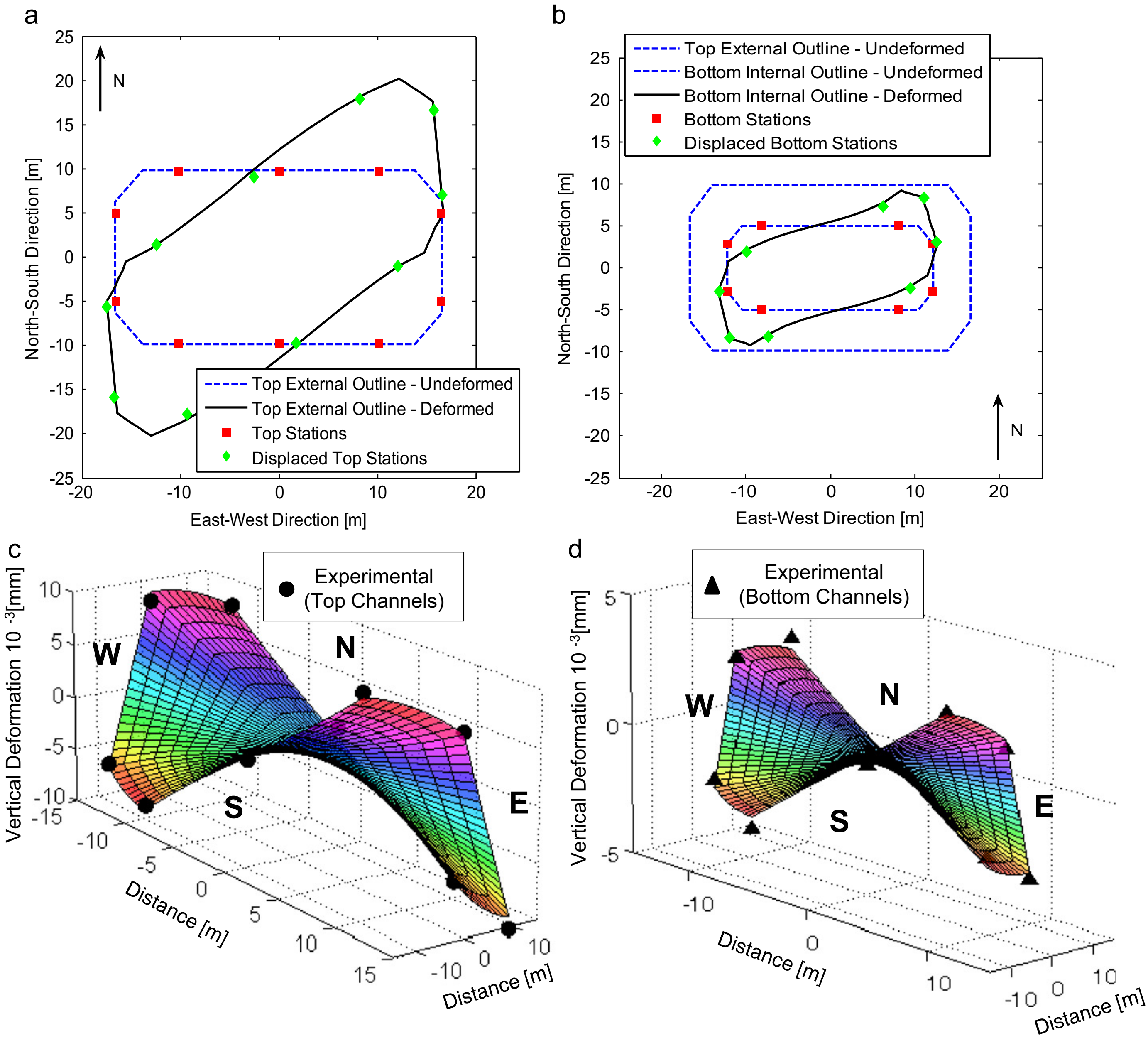

Fig. 19. Displacement and deformation of the reaction block at the top (a) and within (b) the block for torsional excitation at 14.5 Hz, and distribution of vertical displacements on horizontal plane at the top (c) and bottom (d) of the block.

displacements at all 19 stations (jointly). The deformation of a lower level within the block is shown in Fig. 19b. The results in Fig. 19a and b show torsion of the block about a vertical axis and bending of all four walls. In this case, the NS displacements of the East and West walls are similar in amplitude and appear to be less affected by the unfilled soil pit to the east of the block.

The pattern of deformation in the vertical direction is illustrated in Fig. 19c and d, which shows the observed vertical displacements at all 19 stations together with a 5-parameter polynomial interpolation. The results show warping of the block with vertical displacements anti-symmetric with respect to both the NS and EW axes.

6.3. Frequency response functions

After the NEES/UCSD Shake Table is upgraded to 6-DOF, the actuators will exert NS forces on the reaction block, which will lead to an estimated maximum torque about the vertical axis of 41.5 MN m. The results of Test 5 with a total torque of 6.5 MN m at 14.5 Hz were used to estimate the response of the reaction block to a larger torque of 117.5 MN m (2.83 times larger than the expected maximum torque). For this purpose, the recorded accelerations were transformed into displacements and then scaled to an excitation torque of 117.5 MN m independent of frequency by use of the factor $(117.5/6.50)\,(14.5/f)^2/(2\pi f)^2$, where f is the cyclic frequency (Hz). The amplitudes of the resulting NS and vertical frequency response at different locations in the block are presented in Fig. 20a and b, respectively. The amplitudes shown in Fig. 20a correspond to the averages of the NS components:

$T3=(RT4+RT5-RT9-RT10/4$

$T2=(RT3+RT6-RT1-RT8)/4$

$T1=(RT2+RT7)/2$

$B3=(RB3+RB4-RB7-RB8)/4$

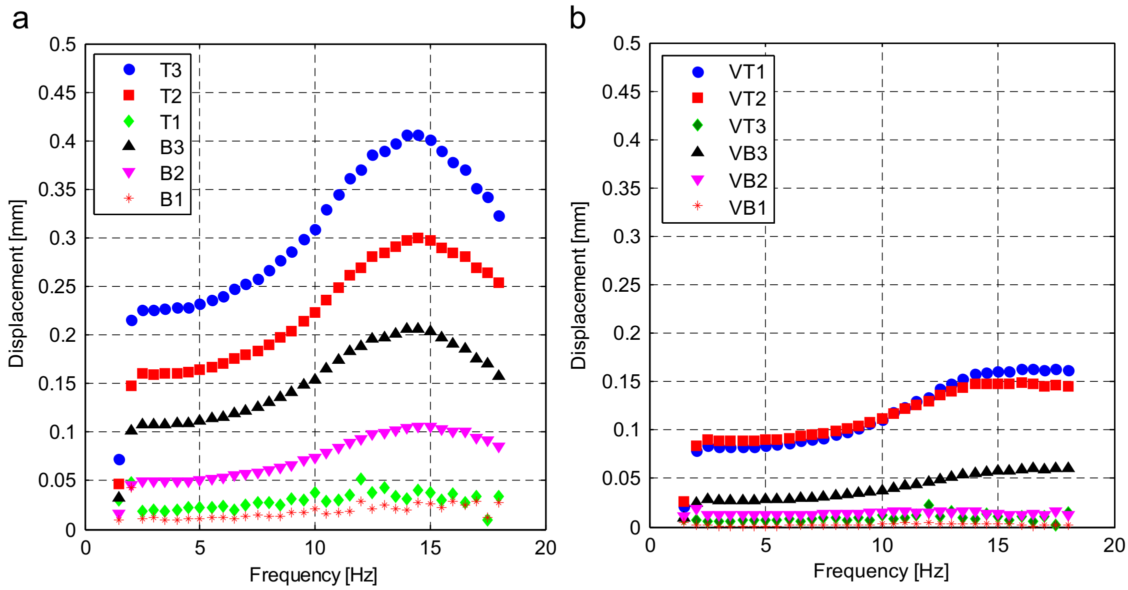

Fig. 20. Scaled amplitudes of the NS (a) and vertical (b) frequency response functions of the reaction block for torsional excitation. The results shown correspond to scaled displacement amplitudes for a harmonic torque of constant amplitude 117.5 MN m.

$$B2 = (RB2+RB5-RB1-RB6)/4$$
$$B1 = RB9 \tag{12}$$

The terms $T1$, $T2$, and $T3$ correspond to average NS motions at the top of the block at symmetric locations with respect to the center of the block. The terms $B1$, $B2$, and $B3$ represent similar averages within the block. The results in Fig. 20a indicate that: (i) the NS frequency response function peaks at 14.5 Hz and has a peak amplification of about 0.41/0.225 = 1.8, (ii) the average displacements increase with distance to the vertical axis of the block indicating a torsional response and localized deformations at the east and west ends of the block, and (v) the NS motions increase with elevation.

The amplitudes shown in Fig. 20b correspond to the averages of the vertical components:

$$VT1 = (RT6+RT1-RT3-RT8)/4$$
$$VT2 = (RT5+RT10-RT4-RT9)/4$$
$$VT3 = (RT7-RT2)/2$$
$$VB3 = (RB5+RB1-RB2-RB6)/4$$
$$VB2 = (RT4+RB8-RB3-RT7)/4$$
$$VB1 = RB9 \tag{13}$$

These averages are based on the assumption that the dominant component of the vertical displacement is anti-symmetric with respect to both the NS and EW axes. The results in Fig. 20b indicate that the amplitudes of the vertical displacements increase with horizontal distance to the EW axis of rotation, and that the peak response occurs at about 18 Hz.

The results in Fig. 20a and b indicate that the maximum scaled horizontal and vertical displacements for the maximum nominal harmonic torque of 41.5 MN m would be 0.15 and 0.06 mm, respectively.

6.4. *Estimates of average rigid-body motion*

The scaled amplitude and the relative phase of the frequency response functions for the average torsional, NS, and rocking (about the x-axis) rigid-body motions of the reaction block subjected to torsional excitation with two shakers with four bricks per basket (Test 5) are presented in Fig. 21. The recorded accelerations during Test 5 were transformed to scaled displacements through multiplication by the factor(117.5/6.50) $(14.5/f)^2/(2\pi f)^2$. The linearly scaled amplitudes correspond to a harmonic excitation torque of 117.5 MN m independent of frequency. The average rigid-body motions were obtained by the least squares approach described earlier (Eq. (5)). The most significant component of the average rigid-body motion is the torsion about a vertical axis. The scaled torsional rigid body motion at the reference point at the top center of the block is consistent with an average of the terms $T1$, $T2$, and $T3$ shown in Fig. 20a for the NS motion of the top of the block. The rocking motion is also consistent with the vertical motion at the north and south walls shown in Fig. 20b. The vertical, longitudinal, and rocking (about the NS axis) components of the average rigid-body motion of the block are very small and are not shown in Fig. 21.

Fig. 21b shows the relative phase of the rocking and NS translational response with respect to the average rigid-body torsional response. The NS response is approximately 60° out of phase with respect to the torsional motion, while the rocking response is approximately 180° out of phase at the excitation frequency of 14.5 Hz.

6.5. *Test of linearity*

The results of Test 5 with a NS force of 0.227 MN per shaker at 14.5 Hz (four bricks per basket) and a total torque of 6.50 MN m at the same frequency, and Test 8 with a force of 0.146 MN per shaker (one brick per basket) and a total torque of 4.18 MN m at 14.5 Hz were used to check the linearity of the system. The recorded accelerations were transformed into displacements and then scaled to an excitation torque of 117.5 MN m independent of frequency. Comparisons of the normalized NS displacements at stations $RT6$ and $RB5$ and of the normalized vertical displacement at station $RT6$ for the two tests are presented in Fig. 22. Fig. 22 shows that there is excellent agreement between the results from the two tests even though the forces (and torques) differ by a factor of 1.56.

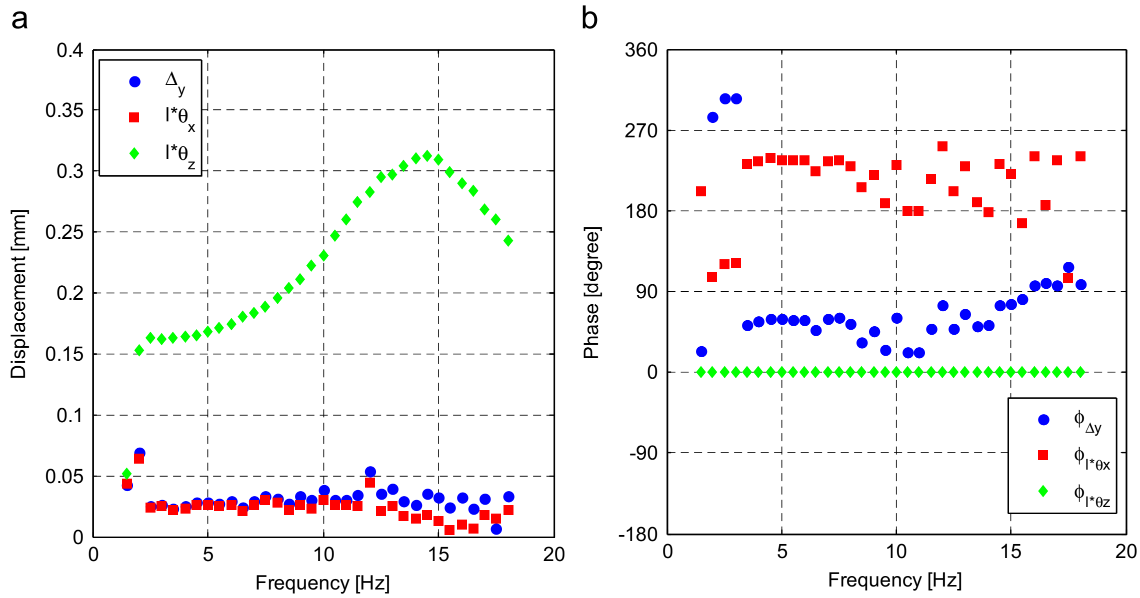

Fig. 21. (a) Scaled amplitude and (b) relative phase of the frequency response function for the average torsional, rocking, and NS rigid-body motion of the reaction block subjected to torsional excitation.

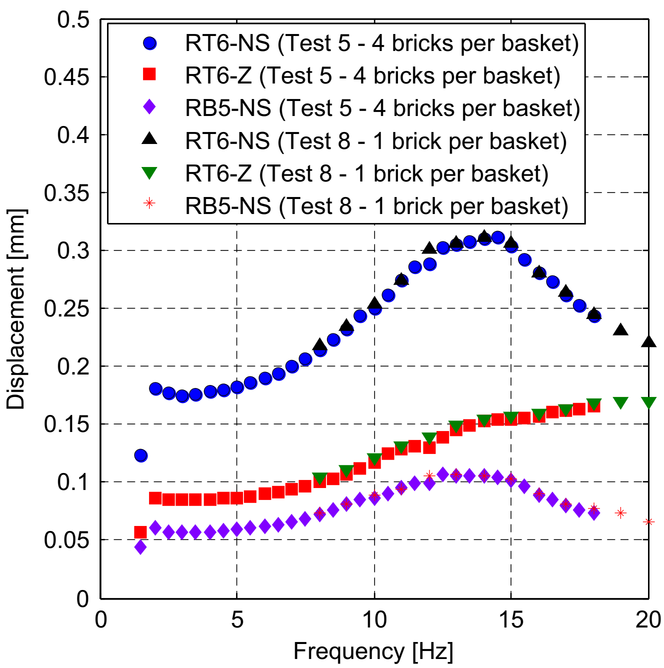

Fig. 22. Test of linearity for torsional excitation based on Tests 5 and 8.

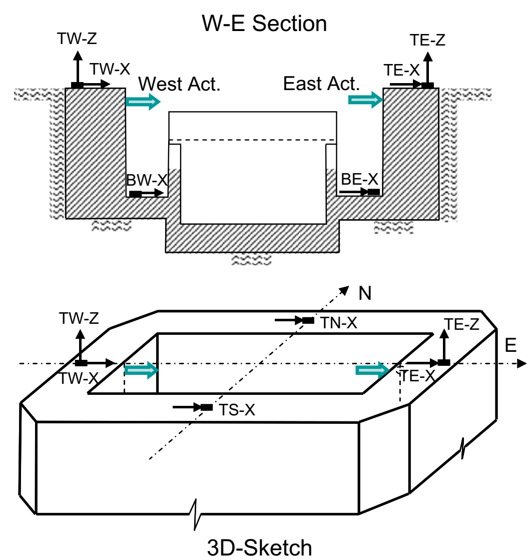

Fig. 23. Locations of accelerometers during harmonic actuator tests SE9–SE16.

7. Comparison of shaker and actuator induced vibrations

During the initial characterization phase of the NEES/UCSD Shake Table, the platen was forced to undergo harmonic motions with frequencies of 4, 6, 8, 10, 12, 14, and 16 Hz (Tests SE9–16). The resulting EW motion of the reaction block was recorded at four stations at the top of the block and at two stations at the base (Fig. 23). The vertical motion of the top of the block was also recorded at the West and East ends of the block. The amplitudes of the total actuator force for tests SE9, SE10, SE11, SE12, SE14, SE15, and SE16 corresponded to 6.38, 6.48, 6.72, 6.67, 5.68, 6.58, and 6.88 MN, respectively. The actuator forces were calculated from the recorded accelerations of the platen and the effective mass of the platen (144,000 kg).

A sample of the accelerations recorded during Test SE12 with a frequency of 10 Hz is shown in Fig. 24. The amplitude of the force acting on the block during this test was 6.67 MN or 98% of the nominal maximum force that the actuators can exert on the platen. The results show that the longitudinal acceleration of the base and the central area at the top of the block reached about 10%g, while the accelerations at the West and East walls reached values of 20%g and 30%g, respectively. The vertical accelerations at the end walls were 180° out of phase and had peak values of 15%g (West) and 25%g (East).

A comparison of the actuator and shaker-induced average rigid-body response of the reaction block during harmonic tests is presented in Fig. 25. The eccentric shaker results correspond to Test 2 with a total force of 0.216 MN at 10 Hz. The amplitudes have been linearly scaled to a force of 6.8 MN, and the rotation angles have been multiplied by the half-length of the reaction block l=16.56 m. The results in Fig. 25 correspond to the scaled amplitudes of the average rigid-body EW and vertical translation at the top of the block (Fig. 25a), and the average rigid-body rocking of the block about the NS axis and torsion about the vertical axis (Fig. 25b). For the results presented in Fig. 25, the components TE-X and TW-X recorded during actuator tests, and those recorded at stations $RT4$, $RT5$, $RT9$, and $RT10$ during the shaker tests, are affected by the local deformation of the end walls of the block, and were not included in the calculation of the average rigid-body motions according to the procedure described in Section 4.3. The relatively good agreement between the two sets of normalized results is encouraging considering that, depending on frequency, the force level during the actuator tests was 13–185 times larger than that during the shaker tests (6.67/0.216 MN = 31 times larger at 10 Hz). In addition, the moments exerted by the two types of forces were not comparable as the shakers exerted a force at an elevation higher than that of the actuators. The results in Fig. 25 confirm that shaker-induced vibrations are a useful tool to study the dynamic response of foundations.

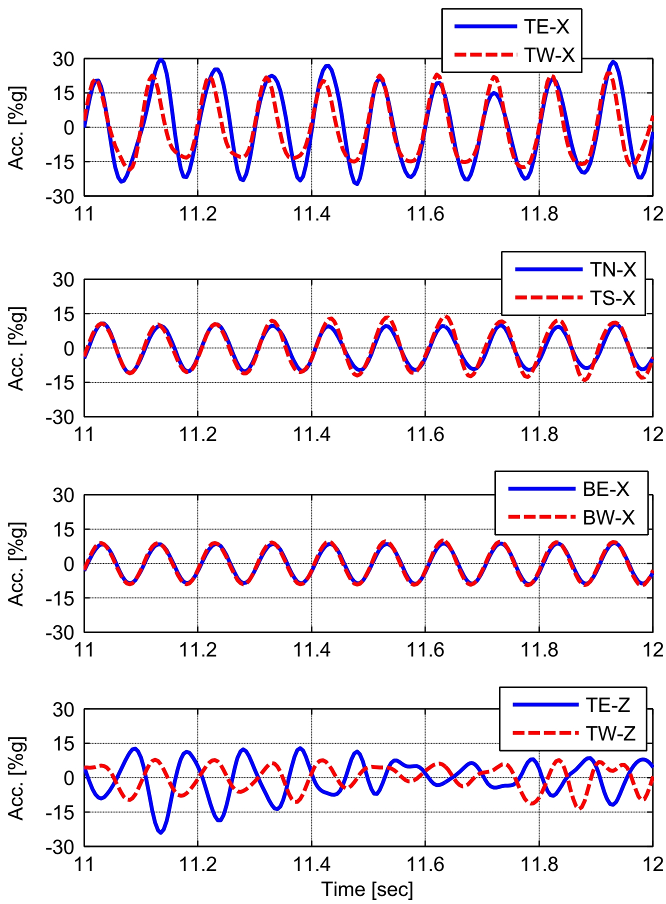

Fig. 24. Sample of acceleration time histories recorded during harmonic actuator Test SE12 at a frequency of 10 Hz.

8. Comparison of experimental and theoretical results

Although a precise comparison of the experimentally obtained response of the reaction block with theoretical results requires consideration of the complex shape of the reaction block and of its flexibility, it is instructive to consider the response of a rigid block with a simplified geometry. The model corresponds to a rectangular block with basal aspect ratio $b_e/c_e = 1.69$, basal area $b_e c_e = 617.2\,\text{m}^2$, and effective embedment depth $h_e = 6.03\,\text{m}$. The basal area with an effective radius $a_e = 14.02\,\text{m}$ considers the missing corners of the reaction block. The effective embedment depth (6.03 m) represents a weighted average of the depth (5.79 m) of most of the foundation and the depth (7.92 m) of the smaller central region. The reaction block model is embedded in a layered soil with the properties illustrated in Fig. 4.

The harmonic translational $(\Delta_{x0}e^{i\omega t})$ and rocking $(\theta_{y0}e^{i\omega t})$ response of the block for a harmonic force $F_s e^{i\omega t}$ acting in the longitudinal direction can be obtained from

$$\left(\begin{bmatrix}\overline{K}_{11} & \overline{K}_{15}\\ \overline{K}_{51} & \overline{K}_{55}\end{bmatrix} - a_0^2 B\begin{bmatrix}1 & (h_G/a_e)\\ (h_G/a_e) & (I_0/Ma_e^2)\end{bmatrix}\right)\begin{Bmatrix}\Delta_{x0}\\ a_e\theta_{y0}\end{Bmatrix} = \left(\frac{F_s}{\overline{G}a_e^2}\right)\begin{Bmatrix}1\\ h_s/a_e\end{Bmatrix} a_e \qquad (14)$$

where $a_0 = \omega a_e/\overline{\beta}_s$ is a dimensionless frequency based on a reference shear wave velocity $\overline{\beta}_s$; $B = M/\overline{\rho}_s a_e^3$ is the normalized

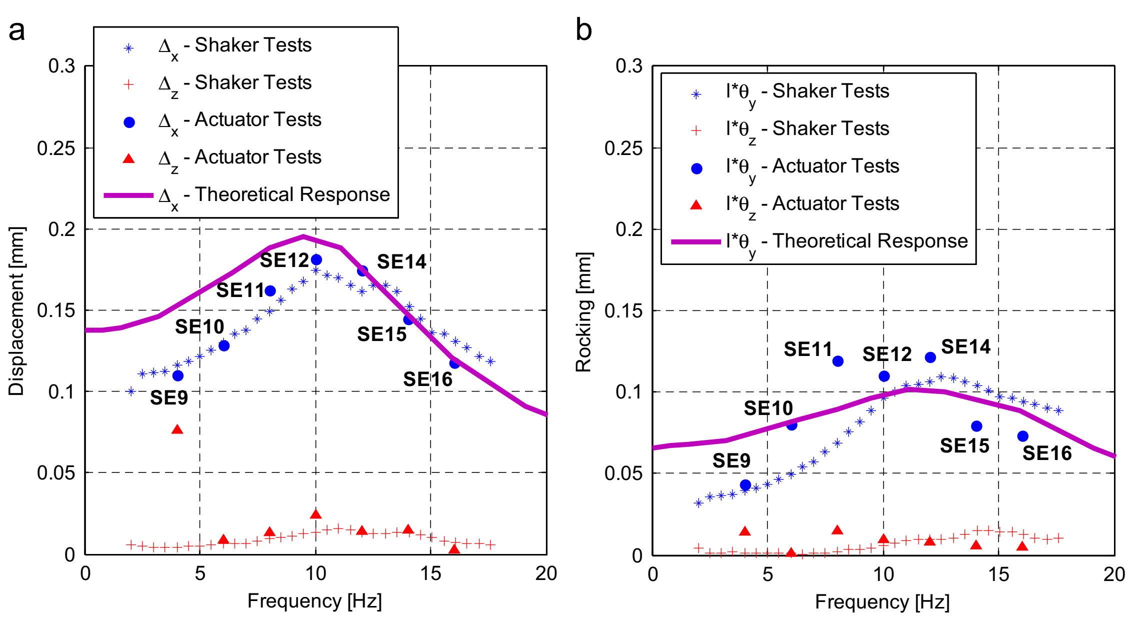

Fig. 25. Comparison of the actuator and shaker-induced response of the reaction block during harmonic tests. (a) Amplitudes of the scaled average rigid-body EW and vertical translation at the top of the block, and (b) amplitudes of scaled average rigid-body rocking and torsion of the block.

mass ratio in which M is the mass of the reaction block and $\overline{\rho}_s$ is a reference soil density; I_0 is the mass moment of inertia of the block with respect to a horizontal axis at the reference depth (6.03 m); h_G is the height of the center of mass of the block with respect to the reference depth; $\overline{G}=\overline{\rho}_s\overline{\beta}_s^2$ is a soil shear modulus of reference; h_s is the height of the point of application of the shaker force; and $\overline{K}_{11}$, $\overline{K}_{15}$, and $\overline{K}_{55}$ are the normalized complex horizontal, coupling, and rocking impedance functions given by

$$\overline{K}_{11}=K_{11}/\overline{G}a_e=k_{11}(a_0)+ia_0c_{11}(a_0) \quad (15a)$$

$$\overline{K}_{15}=\overline{K}_{51}=K_{15}/\overline{G}a_e^2=k_{15}(a_0)+ia_0c_{15}(a_0) \quad (15b)$$

$$\overline{K}_{55}=K_{55}/\overline{G}a_e^3=k_{55}(a_0)+ia_0c_{55}(a_0) \quad (15c)$$

These impedance functions are referred to the reference depth of 6.03 m. Once the translation at the base Δ_{x0} and the normalized rotation $a_e\theta_{y0}$ have been obtained from Eq. (14), the translational Δ_{xT} at the top of the reaction block can be obtained from

$$\Delta_{xT}=\Delta_{x0}+(h_e/a_e)a_e\theta_{y0} \quad (16)$$

After selecting the shear wave velocity of reference $\overline{\beta}_s=560\,m/s$ and the soil density$\overline{\rho}_s=1841\,kg/m^3$, the remaining dimensionless parameters for the block are estimated to be $B=0.867$, $I_0/Ma_e^2=0.564$, $h_G/a_e=0.168$, $F_s/\overline{G}a_e^2=6.01\times10^{-5}$, $h_s/a_e=0.452$, and $h_e/a_e=0.43$.

The impedance functions were estimated by use of existing tables of impedance functions for simple foundation geometries and soil characteristics. The process involved the following steps:

(i) The impedance functions for a rigid rectangular foundation with aspect ratio $b/c=1.69$ resting on the surface of a uniform half-space with a shear wave velocity of 560 m/s was obtained by interpolation of the numerical results presented by Wong and Luco [19] for rectangular foundations with $b/c=1$ and $b/c=2$.
(ii) A correction for the effect of the increase of the shear wave velocity from 560 to 762 m/s at a depth of 11.92 m was introduced by interpolation of the results listed by Wong and Luco [20] for a rigid square surface foundation resting on a layer over an elastic half-space.
(iii) Finally, a correction for embedment depth was included based on the results of Apsel and Luco [21] for a rigid cylinder embedded in a uniform elastic half-space. This correction was modified to account for the softer layers surrounding the foundation and by the fact that there was little effective embedment on the east side of the block as the adjacent soil pit was empty at the time of the tests.

The contributions of the various corrections to the impedance functions for a frequency of 9.55 Hz($a_0=1.50$) are illustrated in Table 3. It can be seen that the main effect of layering corresponds to a reduction of the radiation damping, and to an increase of the

Table 3
Corrections to the stiffness and damping coefficients for layering and embedment (f=9.55 Hz).

	Basic coefficients	Corrections for layering	Corrections for embedment	Corrected coefficients
k_{11}	4.67	−0.02	0.56	5.20
k_{55}	4.67	1.20	0.47	6.34
k_{15}	−0.52	−0.23	0.25	−0.50
c_{11}	2.92	−0.99	0.83	2.76
c_{55}	1.63	−0.66	0.20	1.17
c_{15}	0.18	−0.09	0.23	0.32

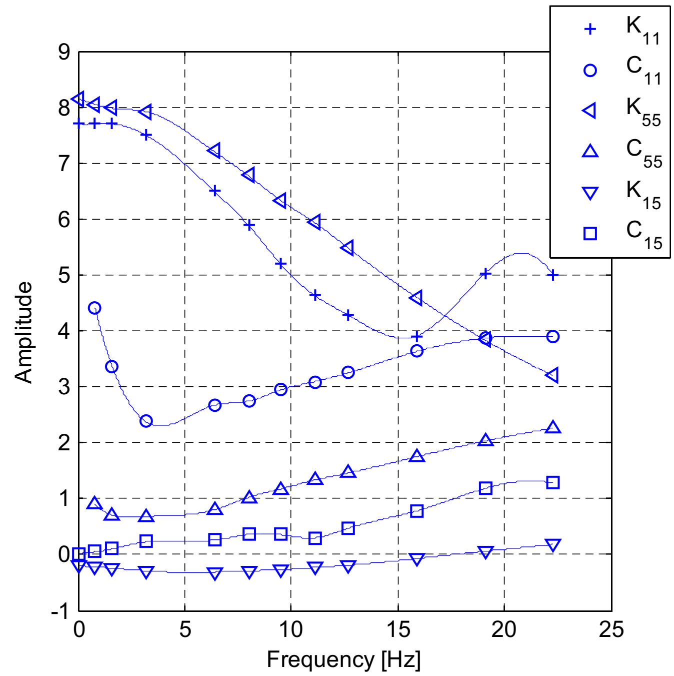

Fig. 26. Normalized impedance functions.

rocking stiffness. The embedment of the block leads to increases of the stiffness and radiation damping coefficients. The estimated stiffness (k_{ij}) and damping (c_{ij}) coefficients obtained by this process are illustrated in Fig. 26.

The amplitudes of the translation at the top of the block $|\Delta_{xT}|$ and the normalized rotation $|l\theta_{y0}|$ ($l=16.56\,$m) calculated by the use of Eqs. (14) and (16) are compared in Fig. 25 with the corresponding components of the rigid-body motion of the block obtained from Test 2. Both sets of results have been scaled to a harmonic force of constant amplitude$F_S=6.8\,$MN. The agreement between the two sets of results is reasonable considering the simplicity of the assumed foundation model and the approximations introduced in the process of estimating the impedance functions.

9. Conclusions

It has been shown again that shaker-induced vibrations are a useful tool to study the dynamic interaction between the foundations and the surrounding soil. In particular, properly scaled shaker-induced vibrations resulted in accurate estimates of the dynamic response of the reaction block of the NEES/UCSD Shake Table during actuator-induced vibrations. Good agreement was found between the two sets of scaled results even though the force levels during the actuator tests were, depending on frequency, 13–185 times larger than the level during the shaker tests (6.67/0.216 MN=31 times larger at 10 Hz). Also, the points of application of the shaker and actuator forces differed in elevation and, consequently, the moments exerted by the two types of forces were not fully comparable.

It has been shown experimentally that the displacements of the reaction block are sufficiently small not to interfere with the control of the shake table. For a harmonic force of 6.8 MN corresponding to the maximum force that the actuators can exert on the reaction block, the average rigid-body translation at the top of the block has amplitude of less than 0.2 mm. The corresponding amplitude of the average displacement at the ends of the West and East walls is 0.26 mm and the displacements at the centers of the West and East walls near the supports of the actuators are 0.42 and 0.64 mm, respectively.

These displacements are a very small fraction of the maximum stroke of the actuators, which is 0.75 m. The controller of the shake table uses the absolute acceleration of the platen and the relative displacement between the platen and the reaction block as feedback to control the motion of the table. The implicit assumption, now validated, is that the relative displacement of the platen is similar to the absolute displacement.

The results obtained validate the unconventional design of the NEES@UCSD foundation block that took advantage of the natural conditions at the site in terms of high soil stiffness to build a lighter and considerably less costly foundation, which resulted in a high characteristic frequency and a large effective (radiation) damping ratio as opposed to the conventional design that relies on the use of massive foundations to achieve a low characteristic frequency. In the longitudinal EW direction, the frequency response curves for a harmonic force of constant amplitude show a broad peak at 10 Hz. Depending on the component considered, the dynamic amplification varies from 1.3 (motion on East and West walls at top of the block) to 1.67 (average rigid-body motion), suggesting an effective damping ratio between 32% and 42%, and a characteristic soil-foundation frequency between 11.2 and 12.5 Hz. These values are somewhat lower than those considered in the initial design for two main reasons: (i) the soil pit immediately adjacent to the reaction block was empty at the time of the tests, and (ii) cost cutting measures resulted in the trimming of the corners of the reaction block (compare Figs. 1 and 5). In addition, there are indications of a deeper and stiffer layer of soil at a depth of about 12 m, which reduces the radiation damping into the soil.

The average rigid-body motion and the deformation patterns of the reaction block for longitudinal (EW), transverse (NS), and torsional excitations of the block have been determined. The deformation patterns show out-of-plane deformation of all four walls and the base slabs. The deformations are more pronounced on the East and West ends of the block, and particularly on the East wall adjacent to the (then) empty soil pit. The coupled translation–rocking rigid-body motion of the block for longitudinal excitation has a peak at 10 Hz and shows a significant rocking component. The rigid-body motion response for symmetric transverse excitation has a coupled translation–rocking component that also peaks at 10 Hz and a torsional component associated with lateral variation of the soil conditions. The torsional response of the block peaks at a frequency of 14.5 Hz. All foundation-soil modes have low dynamic amplification showing a significant amount of radiation damping.

It is hoped that the data presented here will prove helpful in the validation of dynamic, three-dimensional, soil–foundation interaction analysis methods and the associated computer codes. An initial comparison with a simplified model of the foundation indicates that analytical methods can capture most of the experimental response. Data on the dynamic interaction through the soil between the adjacent foundations of the reaction block, control building and blast simulation facility, and on the variation of the motion on the soil surface away from the reaction block will be presented elsewhere.

Acknowledgments

Support of this research by the National Science Foundation under Award No. CMMI-0301785 is gratefully acknowledged. Any opinions, findings, conclusions, or recommendations expressed in this publication are those of the authors and do not necessarily reflect the views of the sponsor. The authors are grateful to Dr. Steve McCabe for his support of the project at NSF. Some of the equipments used in the field program were provided by the PASSCAL facility of the Incorporated Research Institutions for Seismology (IRIS) through the PASSCAL Instrument Center at New Mexico Tech. The facilities of the IRIS Consortium are supported by the National Science Foundation under Cooperative Agreement EAR-0552316 and by the Department of Energy National Nuclear Security Administration.

The technical contributions made by D. Whang, S. Kang, and R. S. Keowen of NEES@UCLA; R. Reyes and E. Rocha of CICESE, Mexico; G. Acero and B. Moaveni of UCSD; and L. Berman of NEES@UCSD during the experimental phase of this large scale study are gratefully acknowledged. F. Vernon of the Scripps Institute of Oceanography at UCSD advised the project PIs on a number of technical issues related to the instrumentation and wireless data acquisition system used in the tests. He also generously translated the extensive Antelope data files into more convenient Matlab files.

References

[1] Ozcelik O, Conte JP, Luco JE. Virtual model of the UCSD-NEES high performance outdoor shake table. In: Proceedings of the fourth world conference on structural control and monitoring, San Diego, California, July 11–13; 2006.

[2] Trifunac MD, Todorovska MI, Hao TY. Full-scale experimental studies of soil-structure interaction—a review. In: Proceedings of the 2nd U.S.–Japan workshop on soil–structure interaction, Tsukuba City, Japan, March 6–8; 2001.

[3] Ozcelik O, Luco JE, Conte JP, Mendoza LH. Experimental study of the dynamic interaction between the foundation of the NEES/UCSD Shake Table and the surrounding soil: soil response. Soil Dynamics and Earthquake Engineering, in preparation.

[4] Prowell I, Veletzos M, Elgamal A, Restrepo JI. Shake Table test of a 65 kW wind turbine and computational simulation. In: *Proceedings of the 14th world conference on earthquake engineering*, October 12–17, Beijing, China; 2008.

[5] Panagiotou M, Restrepo JI, Conte JP. Shake table test of a full-scale 7-story building slice phase I: rectangular wall. Journal of Structural Engineering, American Society of Civil Engineers, in press.

[6] Schoettler MJ, Belleri A, Zhang D, Restrepo JI, Fleischman RB. Preliminary results of the shake-table testing for the development of a diaphragm seismic design methodology. PCI Journal 2009:100–24.

[7] Stavridis A, Koutromanos I, Shing PB. Shake-table tests of a three-story reinforced concrete frame with masonry infill walls. Journal of Earthquake Engineering and Structural Dynamics, in preparation.

[8] Okail H, Shing PB, Klingner RE, McGinley WM. Performance of clay masonry veneer in wood-stud walls subjected to out-of-plane seismic loads. Journal of Earthquake Engineering and Structural Dynamics 2010.

[9] Wilson P, Elgamal A. Full-scale shake-table investigation of bridge abutment lateral earth pressure. Bulletin of the New Zealand Society Earthquake Engineering 2009;42(1):39–46.

[10] Geocon Inc., Geotechnical Investigation, Structure Testing Facility, Elliot Field Station, University of California, San Diego, California. Report, April 19; 2002.

[11] Ashford S. Personal communication.

[12] Ozcelik O, Luco JE, Conte JP, Trombetti TL, Restrepo JI. Experimental characterization, modeling and identification of the NEES-UCSD shake table mechanical system. Earthquake Engineering and Structural Dynamics 2008;37:243–264.

[13] Ozcelik O, Luco JE, Conte JP. Identification of the mechanical subsystem of the NEES-UCSD shake table by a least-squares approach. Journal of Engineering Mechanics, ASCE 2008;134(1):23–34.

[14] Van Den Einde L, Restrepo JI, Conte JP, Luco JE, Seible F, Filiatrault A, Clark A, et al. Development of the George E. Brown, Jr. network for earthquake engineering simulation (NEES) large high performance outdoor shake table at the University of California, San Diego. In: Proceedings of the 13th world conference on earthquake engineering, Vancouver, B.C., Canada August 1–6, Paper No. 3281; 2004.

[15] Conte JP, Luco JE, Restrepo JI, Seible F, Van Den Einde L. UCSD-NEES large high performance outdoor shake table. In: Proceedings of the 17th ASCE engineering mechanics conference. Newark, DE: University of Delaware, June 13–16; 2004.

[16] Stewart JP, Whang DH, Wallace JW, Nigbor RL. Field testing capabilities of the NEES@UCLA equipment site for soil–structure interaction applications. In: Boulanger RW, Deewolder M, Gucunski N, Juang CH, Kalinsky ME, Kramer SL, Manzari M, Pauschke J, editors. Earthquake engineering and soil dynamics, Proceedings of sessions of the geo-frontiers 2005 congress, *ASCE Geotech. Special Publication 133*, 9 pages (electronic file); 2005.

[17] Keowen RS. personal communication.

[18] Boulder Real Time Technologies. Antelope release 4.8. 〈http://www.brtt.com〉; Boulder Real Time Technologies, Inc., Boulder, Colorado.

[19] Wong HL, Luco JE. Tables of impedance functions and input motions for rectangular foundations. Report CE 78-15. Los Angeles, California: Department of Civil Engineering, University of Southern California; 1978.

[20] Wong HL, Luco JE. Tables of impedance functions for square foundations on layered media. Soil Dynamics and Earthquake Engineering 1985;4(2):64–81.

[21] Apsel RJ, Luco JE. Impedance functions for foundations embedded in a layered medium: an integral equation approach. Earthquake Engineering and Structural Dynamics 1987;15(2):213–231.